ENERGY LOSS TO THE SOIL SURROUNDING A BELOW-GRADE SOLAR ENERGY STORAGE POND

by

Brian James Holmes

Dissertation submitted to the Graduate Faculty of the Virginia Polytechnic Institute and State University in partial fulfillment of the requirements for the degree of

DOCTOR OF PHILOSOPHY

in

Environmental Sciences and Engineering

APPROVED:

J. P. Mason, Jr., Chairman

H. A. Hughes

H. L. Moses

C. W. Randall

D. H. Vaughan

April, 1979

Blacksburg, Virginia

ACKNOWLEDGEMENTS

The work upon which this dissertation is based was supported in part by a grant from the U.S. Department of Agriculture - Science and Education Administration (Cooperative Agreement Number 12-14-7001-557).

The author wishes to express gratitude to the Agricultural Engineering Department and Dr. D. H. Vaughan for their support and also to the follcwing people: Dr. H. A. Hughes and Dr. J. P. Mason for their encouragement and understanding; Dr. C. W. Randall and Dr. H. L. Moses for serving on my Graduate Committee and reading my thesis; J. D. C. Baldwin for his assistance in developing data acquisition equipment; J. C. Carr and Dr. V. O. Shanholtz for their invaluable advice on computer programming techniques; the VPI & SU Swine Center personnel for their cooperation and assistance; Dr. G. W. Cole and Dr. M. P. Kamat for the time they spent in problem discussion sessions with me; for her excellent typing skills and sacrificed weekends; and finally, my loving wife, , without whose patience and hard work this manuscript would not have been completed.

TABLE OF CONTENTS

LIST OF TABLES

LIST OF FIGURES

INTRODUCTION

Production agriculture consumed 2.8 percent of the United States total energy budget in 1974 (U.S. Department of Agriculture, 1976). Twelve percent of the energy used in production agriculture was consumed by the livestock, dairy, and poultry industries, while 8 percent was used in crop drying (U.S. Department of Agriculture, 1976). The 2.8 percent of the total energy budget represents 18 percent of the energy required to produce, process and deliver food to the family table (CAST, 1977). It is apparent that the energy necessary for agricultural production is relatively small compared to total consumption. However, without sufficient energy inputs to production agriculture, yields would be reduced and the well being of many Americans would suffer.

Recent rapid increases in the cost of fossil fuels stimulated renewed interest in the utilization of solar energy. The most promising techniques for exploiting solar energy for production agriculture are in the areas of space heating, crop drying, and wash water heating. These uses constitute a large proportion of the energy requirements for animal production. Solar energy can be used for these purposes because the energy does not have to be transported

long distances from where it is collected to where it is used. Also, temperature of the energy transport medium can be relatively low, thus increasing collection efficiency and reducing transport losses.

If maximum benefit is to be gained from solar energy, a portion of it must be stored for use during periods when immediate collection is not possible. One problem encountered when designing solar energy systems is providing effective low-cost energy storage. Several techniques have been proposed for storing collected solar energy. Most energy storage devices exploit the heat capacity of the heat storage material. In principle, the energy stored in or removed from the material is proportional to the heat capacity of the material, the difference in the temperature before and after the energy change and the mass of the material being considered. Mathematically this can be expressed as

$$\begin{bmatrix}\text{Energy}\\ \text{Change}\end{bmatrix} = \begin{bmatrix}\text{Heat}\\ \text{Capacity}\end{bmatrix} \begin{bmatrix}\text{Material}\\ \text{Mass}\end{bmatrix} \begin{bmatrix}\text{Temperature}\\ \text{Before}\end{bmatrix} - \begin{bmatrix}\text{Temperature}\\ \text{After}\end{bmatrix} \quad [1]$$

The most common materials for energy storage are water and rock. Water is one of the best materials that can be used as an energy storage medium because of its inherently high heat capacity, 4.18×10^3 J/kg-^{0}C (1 BTU/lb-^{0}F). Crushed

rock, on the other hand, has a lower heat capacity which is on the order of 0.84 x 10^3 J/kg-^{0}C (0.2 BTU/lb-^{0}F). However, its porous nature allows heat transfer fluids to be moved through it quite easily. The main attraction of these two materials is their relatively low cost and ready availability.

Conventional energy storage devices, which utilize water as the storage medium, employ a tank to contain the water. Tanks may be free standing or buried. In either case, purchase and installation of tanks adds appreciably to the cost of a solar energy heating system, especially when large capacity tanks are needed. Consequently, lower cost containers are being considered as energy storage devices. By utilizing a container for more than one purpose, the cost can be reduced and the need for extra containers eliminated. For example, animal production facilities that might use solar energy frequently have a stock watering pond, wastewater lagoon, waste holding tank or pit, or a cistern that could also be used as an energy storage device.

For an energy storage device to be effective, energy losses must be kept within an acceptable range. To accomplish this, proper insulation must be provided to reduce heat transfer from the energy storage medium to the surroundings. Insulation can be provided along the walls

and bottom of a container fairly easily during construction, but retroactive insulation of container walls is often impossible. Consequently, this investigation considered insulation of the container walls as well as other means of insulation that would reduce energy losses into the soil.

An energy storage pond was selected for this study. To promote pond wall stability, the walls of the pond were sloped. The resulting shape of the pond (inverted truncated pyramid) made it extremely difficult to find a heat transfer relationship that can be considered an "exact solution" to the differential equation of heat transfer for the pond. Consequently, the finite element method was selected as an effective approximate solution to the differential equation of heat transfer from the pond.

OBJECTIVES

The objectives of this study are enumerated as follows:

1. Develop a three dimensional model capable of predicting soil temperatures in the vicinity of a solar energy storage pond. This model must have the capability to deal with such factors as variations in weather conditions, storage pond water temperature and quantity, and location of insulation that may be installed next to the soil.
2. Implement the model developed in objective 1 with the aid of a computer program.
3. Construct and instrument a warmed water storage pond and collect weather data to be used in the model and in validation of the model output.
4. Use the model to evaluate the influence of various parameters on the energy losses from the energy storage pond.
5. Make recommendations concerning the location of insulation.

LITERATURE REVIEW

The recent rebirth of interest in the use of solar energy has aroused concern as to how excess collected energy can be stored. One technique for storing excess energy entails a warmed medium contained in a below grade structure. Since the storage of heat energy has not been of primary concern in the past, very little research has been done on the storage of energy in below grade structures. The following paragraphs discuss some of the limited information that has been learned about energy losses from below grade energy storages.

Shelton (1975) developed a computer model to study heat losses from a buried hemispherical energy storage. This storage was assumed to have conduction losses to the soil. At an infinite distance from the storage device, the soil temperature was assumed to be unaffected by the temperature of the pond. He concluded the following: 1) Heat loss to the surrounding ground is "only a few percent of the heat storage capacity for a typical home-size unit in low conductivity ground in the absence of liquid-water flow. The economics of added insulation under these circumstances appears to be critically site and system specific".

2) "The time required for the average heat loss rate of a new system... to approach the steady-state value is on the order of a year." 3) "The ground surrounding a typical heat-storage facility contributes very little to the system's storage capacity either on a daily or a seasonal basis."

Beard, et. al. (1977) developed an analog model of a hemispherical pool in the ground with the water surface at the same elevation as the ground surface. In testing the model using water at 82 °C (180 °F) with and without the assumption of insulation at the soil-air interface, they found the energy losses to be 1.7 times as high without insulation as with insulation. These authors have also developed a digital model which gives results similar to those obtained with the analog model.

Stickford, Holt, and Whitacre (1976) experimented with a modified version of a soil behavior model developed by Battelle Columbus Laboratories. They simulated an cylindrical tank buried beneath a constant temperature house located in Madison, Wisconsin. They concluded that tank energy losses were 45% greater in mid-winter than in mid-summer. They also concluded that, by assuming moist soil in the vicinity of the tank, energy losses were twice as large as those obtained assuming dry soil.

Misra and Keener (1978) investigated heat loss from a buried energy storage tank containing warmed water. The study involved a mathematical model where energy losses to the soil were in one case assumed as zero and, in the second case, were allowed to occur by conduction to dry soil in the top 0.9m (3 ft) and wet soil below that depth. Their results showed that, when energy losses from the buried tank were allowed to occur, the stored energy was 75.8% less than when perfect insulation assumptions were made. They concluded that the soil does not act as an added energy reservoir giving up energy to the tank when the tank water temperature is lower than that of the surrounding soil. In fact, they asserted that "...analysis at this stage indicates that the surrounding soil is behaving like a heat sink".

Short, Boller, and Badger (1976) constructed a salt gradient solar pond covered with a greenhouse structure. The pond was lined with a plastic film and the sides were insulated. The pond bottom received a layer of coarse sand that was expected to dry out forming an insulating layer after about one half year of operation. They found that this drying did not occur during the first year of operation. They also found the peak pond temperature to be closely related to weekly average ambient air temperature.

Nielson (1976) constructed an uncovered salt gradient solar pond with thermocouples located to a depth of 1 m (3.28 ft) below the pond bottom. He found temperatures to be distributed in an isothermal pattern with temperatures at the 1 m (3.28 ft) depth below pond bottom to be 6 °C (10.8 °F) warmer in May than in January and 14 °C (25.2 °F) warmer in June than in January. The highest pond temperatures were about 60 °C (140 °F) in June.

Holmes, Vaughan, and Bell (1978) have reported the overall results of four pond insulation treatments on heat losses to the soil and air using a relatively constant pond temperature of 20 °C (68 °F). They found that 90% of the energy lost from an uninsulated pond occurred at the air-water interface. Ten percent of the energy was lost to the soil. The uninsulated pond lost energy at 10.4 times the rate of the totally insulated pond. Table 1 summarizes information obtained on energy losses into the soil from energy storage ponds.

Table 1: Summary of Pond Energy Losses to the Soil

Description	Pond Temp. °C (°F)	Energy Loss MJ/m²-day (BTU/ft²-day)	Ref.
3.57 m radius hemispherical pool, insulated ground-air interface, model= theory	82 (180)	2.92 (256.8)	Beard, et.al. (1977)
4.66 m radius hemispherical pool insulated ground-air interface, model= theory	82 (180)	1.87 (164.8)	Beard, et.al. (1977)
4.66 m radius hemispherical pool, insulated ground-air interface, model= analog	82 (180)	1.91 (168.0)	Beard, et. al. (1977)
4.66 m radius hemispherical pool, uninsulated ground-air interface, model=analog	82 (180)	3.28 (288.5)	Beard, et.al. (1977)
7.32 m square water surface dimension truncated pyramid, insulated ground-air interface, model=digital	82 (180)	3.53 (310.6)	Beard, et. al. (1977)
1.37 m radius hemispherical pond, insulated ground-air interface	77 (170)	3.65 (321.6)	Shelton (1975)
3.35 m square water surface dimension, truncated pyramid, measured energy	20 (68)	1.19 (104.6)	Holmes, Vaughan, and Bell (1978)

MATERIALS AND METHODS

An investigation of the most appropriate method for insulating a solar energy storage pond was to be conducted with a mathematical model. For this model to be validated, a physical model was needed. The instrumented model would provide any initial data that might be used in the mathematical model as well as data necessary to verify the mathematical model.

Experimental Ponds

During the summer and fall of 1977, four ponds were constructed at the VPI & SU Swine Center. The ponds were excavated in the shape of an inverted truncated pyramid as close as possible to the specifications of Figure 1. Three of the ponds received separate insulation treatments, while the fourth received no insulation and was considered a control. The insulation treatments are described in Table 2 and Figure 2.

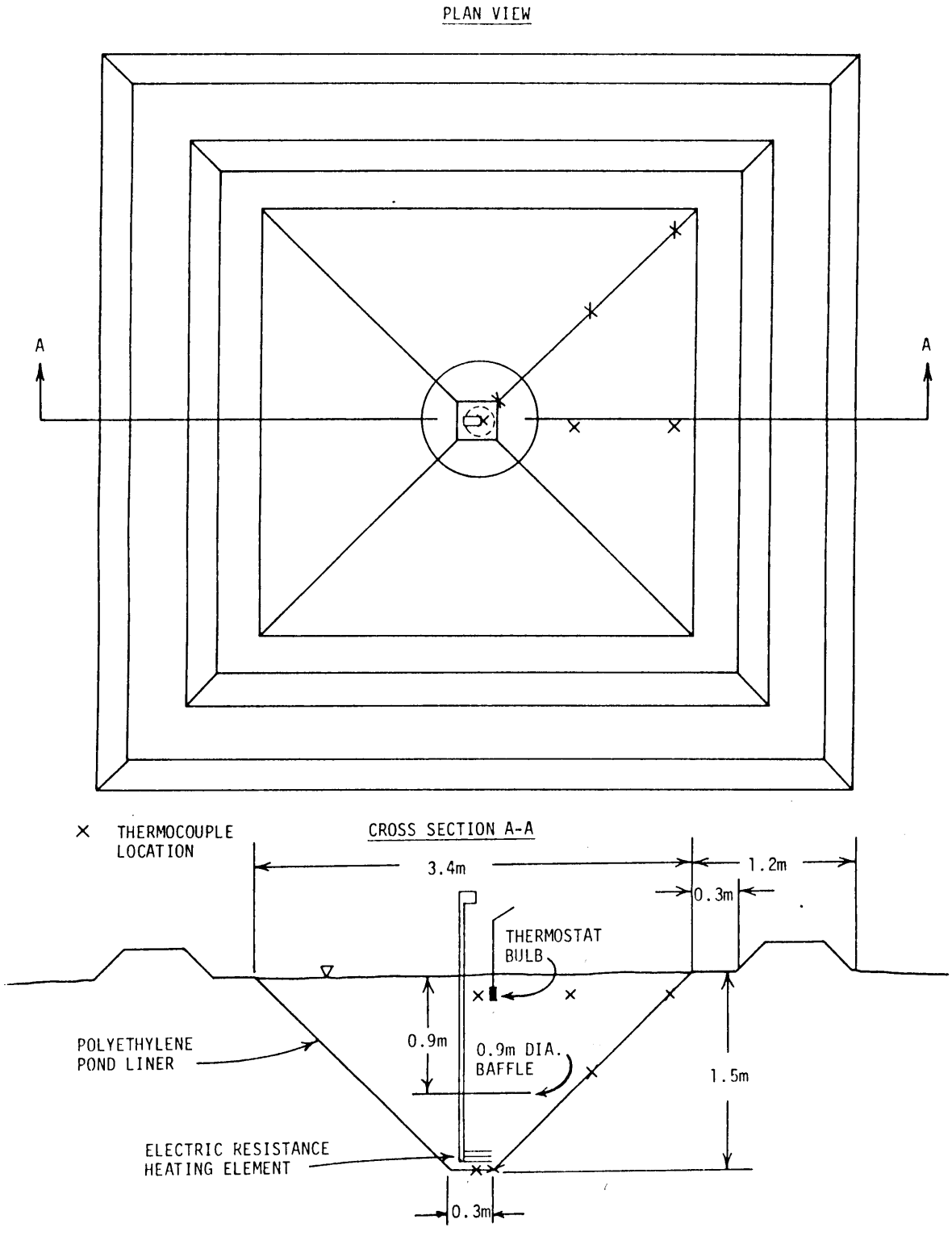

FIGURE 1 PLAN AND CROSS SECTION VIEWS OF UNINSULATED POND #2

Table 2: Insulation and Heater Size for Four Experimental Ponds

Pond Number	Insulation	Resistance Heater Size (kW)
1	Water Surface Insulation Only	6
2	No Insulation	15
3	Water Surface, Side, and Bottom Insulation	2
4	Side and Bottom Insulation	12

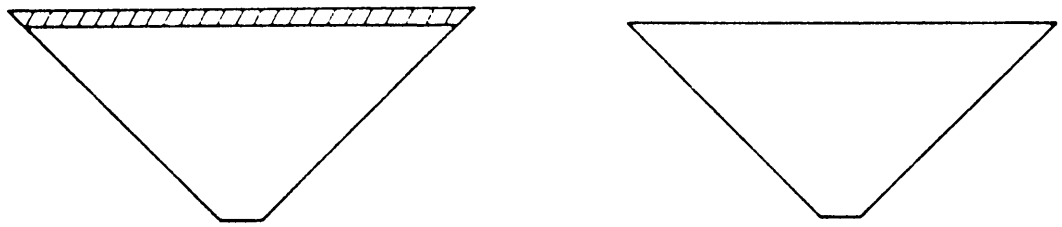

POND 1

TOP INSULATED

POND 2

NO INSULATION

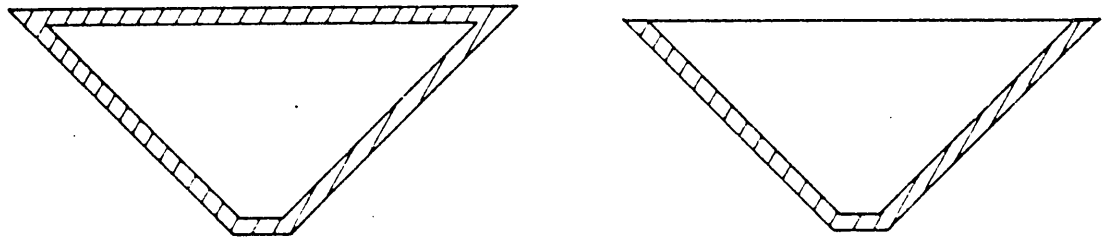

POND 3

TOTAL INSULATION

POND 4

SIDES AND BOTTOM
INSULATED

FIGURE 2 POND INSULATION TREATMENTS

The insulation used in the experiment was 10.2 cm (4 inch) thick rigid board urethane with a heat flow resistance rating of R-21. The insulation for the pond sides and bottom was cut to match the pond shape and was placed in direct contact with the soil. The insulation used on the pond surface was cut to fit the shape of the pond and was floated on top of the water in an alternating joint pattern designed to minimize shifting of the insulation.

The soil at the Swine Center is brecciated with an open structure which, although it is a clay, allows water to pass through it rapidly. To prevent water leakage each pond was lined with a 0.3 mm (10 mil) polyvinyl film. Where the pond bottom and sides were insulated, the plastic film was installed over the insulation to keep the insulation from floating. To secure the edge of the film at the top of the pond, it was placed in a narrow trench and covered with soil.

Each pond was equipped with an electric resistance immersion heater sized to match the estimated energy loss from the pond. The estimated energy losses were calculated using standard heat transfer equations and assumptions of extreme weather conditions (Kreith, 1965). The sizes of heaters placed in the ponds are listed in Table 2. In an attempt to minimize warmed water rising directly to the pond

surface and to obtain better mixing of the warmed water, a 0.76 m (2.5 ft) diameter sheet metal baffle was suspended above each heater. The baffles were suspended about 0.76 m (2.5 ft) above the pond bottom.

Each immersion heater was controlled by a remote bulb thermostat with an approximate differential of 0.5-1.1 °C (1-2 °F) . The remote bulb was located in the center of the pond at a depth of approximately 17.8 cm (7 inch) below the water surface as shown in Figure 1. A wiring diagram for a typical pond heater is shown in Figure 3. The power consumption of each heater was metered, and the meter readings were recorded at least once each day.

Water temperature measurements in the ponds were made with copper/constantan thermocouples located as shown in Figure 1. Thermocouples used to measure pond wall temperature were placed below the plastic film and were not in contact with the pond water. The thermocouples located in the pond water were placed approximately 17.8 cm (7 inch) below the full pond surface.

To provide data for the model and its validation, pond number 2 was more thoroughly instrumented with thermocouples. Before the plastic liner was installed, 7.6 cm (3 inch) diameter holes were augered into the bottom and side of the pond. Holes were also augered beyond the

confines of the pond along a line perpendicular to one of the pond sides and along a line passing through one of the pond corners (Figure 4). Thermocouples were placed into each of these holes to measure soil temperatures in the vicinity of the pond, as depicted in Figure 5.

After the thermocouples were placed into an auger hole, a soil-water mixture was poured into the hole to insure good soil-thermocouple contact. Three thermocouples were also placed below the plastic film in the pond corner, as shown in Figure 4. All thermocouple junctions placed in the soil or water were coated with an ABS plastic pipe cement to reduce the possibility of junction corrosion.

Solar energy data was collected with an Eppley pyranometer which was mounted on a flat plate solar collector stand which was faced due south and tilted 52 degrees from the horizontal. The pyranometer output was integrated with an Esterline-Angus Integrator to obtain the average solar insolation for the period between readings.

The temperature values provided by the thermocouples and the integrated pyranometer output were recorded by an Esterline-Angus PD 2064 data acquisition system.

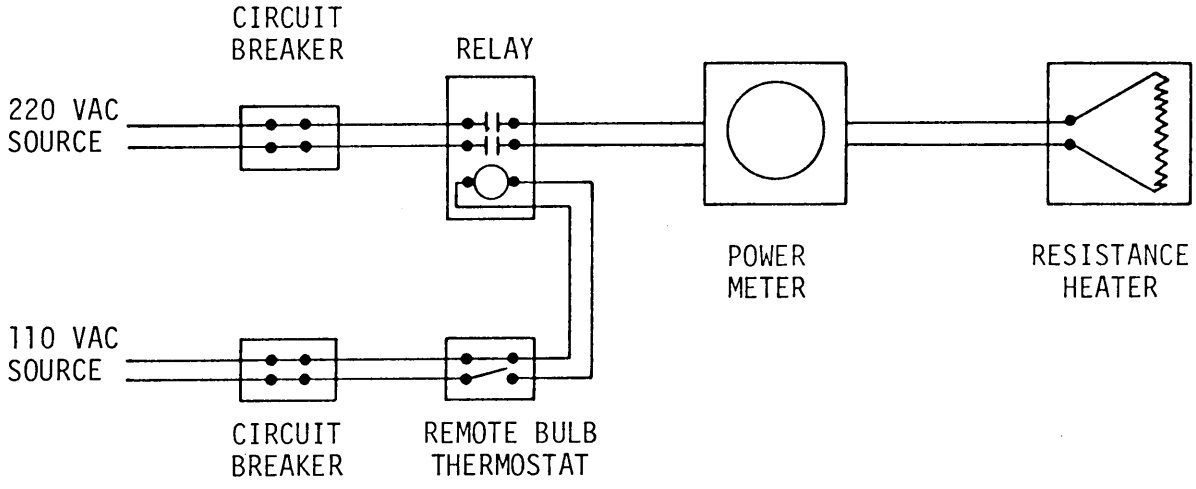

FIGURE 3 WIRING DIAGRAM FOR TYPICAL POND HEATER

X PLAN VIEW OF AUGER HOLE LOCATIONS

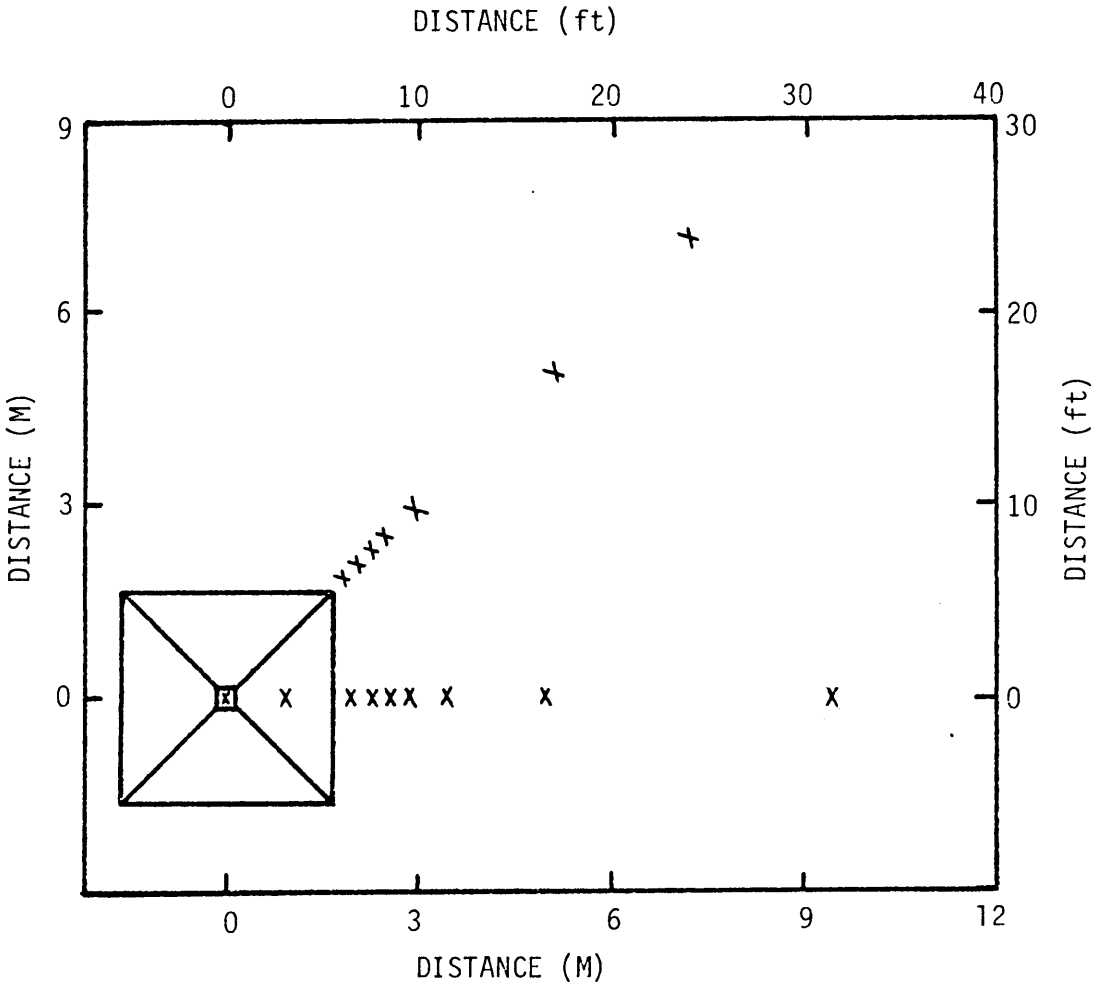

FIGURE 4 PLAN VIEW OF POND OPENING SHOWING AUGER HOLE LOCATIONS

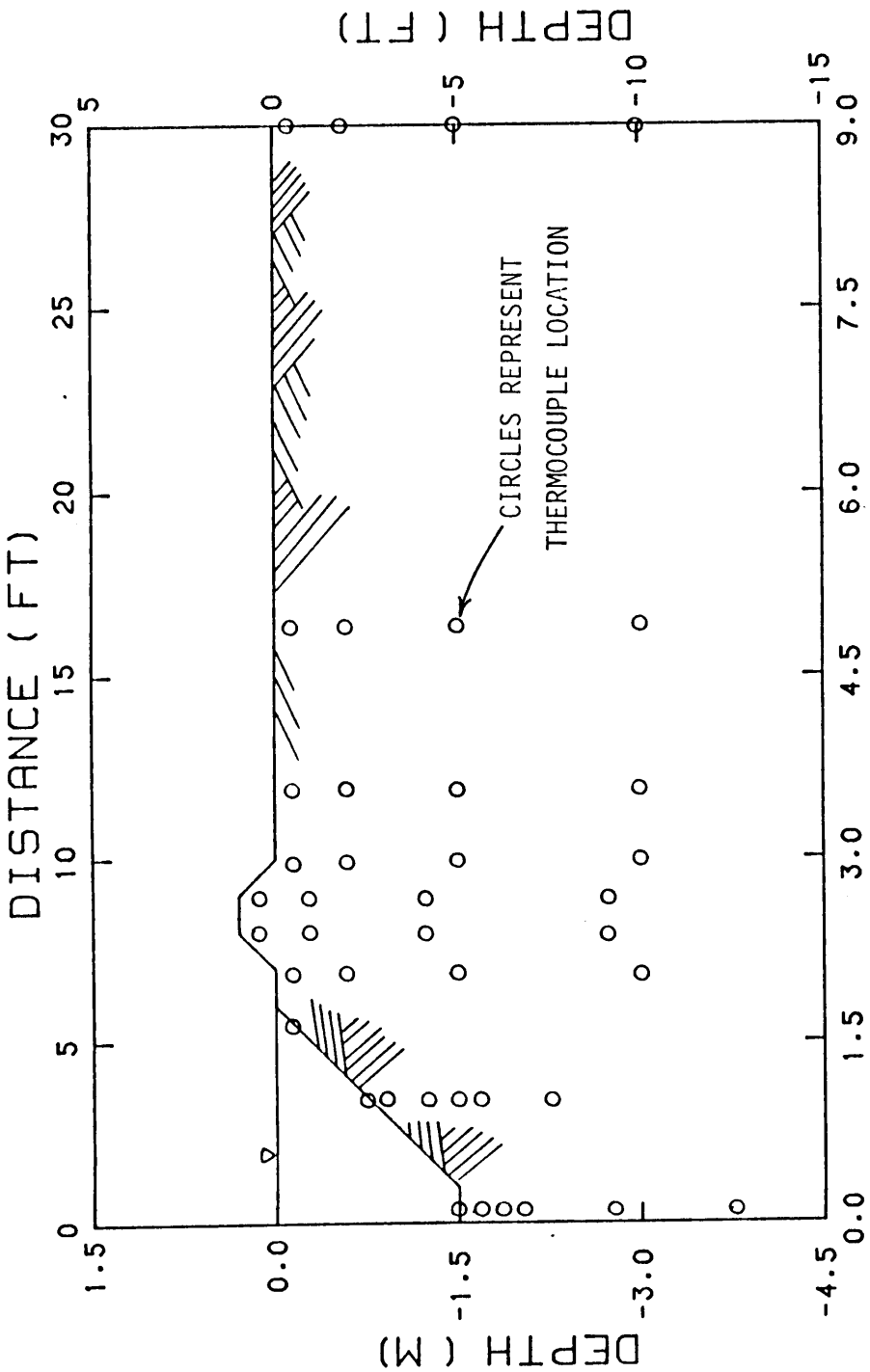

FIGURE 5 POND CROSS SECTION WITH THERMOCOUPLE LOCATIONS

The readings were stored in the system's memory unit and then displayed on its printer and transferred to a cassette magnetic tape through a Texas Instruments Silent 733 data terminal. When sufficient data was stored on magnetic tape, it was transferred to data storage facilities provided by the VPI & SU Computing Center.

Computer Program - General Description

The computer solution of this problem was divided into four programs which are described in the following sections. Copies of each of these programs can be obtained from the Reading Room in the Agricultural Engineering Department at VPI+SU.

Program 1

Program 1 discretized the region in the vicinity of the pond into finite elements and established their respective nodes. The size and shape of the elements were controlled by the input data. The input data were used by the program to determine the location of imaginary rectangular prisms or blocks in the region of the energy storage pond. Each block

was subdivided into six tetrahedral elements. Nodes and elements formed outside of the domain of the soil surrounding the pond were cancelled, thus allowing the shape of the pond and the surrounding soil to be closely approximated by the elements. The shape of the pond dictates that the blocks used in the immediate vicinity of the pond be no larger than a 0.33 m (1 ft) cube in order to adequately approximate the pond shape. This limitation restricted the dimensions of adjoining blocks used in the discretization process to a 0.33 m (1 ft) square face.

Program 2

Program 2 displayed the location of each node with the normal computer print train characters to assure that nodes were formed in the proper locations. Next, Program 2 read soil temperature values that had been measured by the thermocouples (see previous discussion and Figures 4 and 5) and, based on a linear interpolation, developed the assumed initial temperatures at the nodes established by Program 1.

Program 3

This program determined which elements and nodes were

associated with the soil surface-atmosphere interface. The program calculated the surface area for each surface node and the exposed surface area for each surface element. This information was necessary when establishing boundary conditions in Program 4.

Program 4

Program 4 was the main portion of the computer model. It utilized information produced by the other three programs as input data and used the finite element method to calculate nodal temperatures at the end of each time step. When the temperatures were established, the heat transfer from the pond for each time step was calculated and accumulated for the time interval being tested.

This program was developed from basic principles to more completely satisfy the needs of this study. However, the routine that solved the set of simultaneous nodal equations was a slightly modified version of a VPI & SU Computing Center library program from the Scientific Subroutine Package.

Equations of Time Dependent Heat Transfer in Three Dimensions

Many heat transfer relationships that have been modeled involve an "exact" mathematical solution to the problem. Unfortunately exact solutions are usually limited to simple shaped continua such as walls, spheres, cubes, or other specific shapes. The exact solutions are limited by shape because mathematical coordinate systems are usually an integral part of the solution process. For these reasons, a solution procedure for heat transfer from a solar energy storage pond was sought which was capable of dealing with the complex shape of the pond. The finite element method was selected because it could be used to solve for the field variable, temperature, within a complex shaped region. It was also capable of dealing with the boundary conditions that would be imposed on the region. A development of the general finite element method is presented in the appendix. Reference will be made to this development as the time dependent heat transfer equations are discussed.

The governing partial differential equation for time dependent heat conduction within the domain of the volume of

a solid according to (Segerlind,1976) is

$$K_x \frac{\partial^2 T}{\partial x^2} + K_y \frac{\partial^2 T}{\partial y^2} + K_z \frac{\partial^2 T}{\partial z^2} + Q = \lambda \frac{\partial T}{\partial t} \qquad [2]$$

T = temperature

K = thermal conductivity in the x, y, or z direction

Q = internal heat generation, positive for addition of heat

λ = volumetric heat capacity of the material

t = time

At the boundary of the solid, heat transfer can be specified in terms of convection heat transfer or as a known heat flux. This relationship is given as

$$K_x \frac{\partial T}{\partial x} n_x + K_y \frac{\partial T}{\partial y} n_y + K_z \frac{\partial T}{\partial z} n_z + h(T - T_\infty) + q = 0 \qquad [3]$$

T = unknown boundary temperature

K = thermal conductivity in x, y, or z direction

n = direction cosine of the outward normal vector to the boundary surface in the x, y, or z

direction

h = convection heat transfer coefficient

T_∞ = known temperature of fluid surrounding the body at some infinite distance

q = specified heat flux from the surface

The soil in the vicinity of the solar energy storage pond is the domain through which energy is flowing. It is within this region that the model formulated finite elements. The temperature distribution within the soil represents a field which can be described by a function. In the general finite element formulation (appendix) this function was represented as $\{\phi\}$. The functional to be minimized that defines the heat transfer for the system is

$$I(T) = \int_V \left[\frac{K_x}{2} \left(\frac{\partial T}{\partial x}\right)^2 + \frac{K_y}{2} \left(\frac{\partial T}{\partial y}\right)^2 + \frac{K_z}{2} \left(\frac{\partial T}{\partial z}\right)^2 - \left(Q - \lambda \frac{\partial T}{\partial t}\right) T \right] dV + \int_S \left(qT + \frac{h}{2} T^2 - hT\, T_\infty \right) dS \qquad [4]$$

For $I(T)$ to be minimized over one element, the partial derivative of the functional with respect to temperature at all nodes of the element must be zero or

$$\frac{\partial I(T)}{\partial T_m} = 0 \qquad m = 1, 2, 3 \ldots\ldots r \qquad [5]$$

Thus, for a typical node m the partial derivative of the

functional for an element becomes

$$\frac{\partial I(T^e)}{\partial T_m} = 0 = \int_V \left[K_x \frac{\partial T^e}{\partial x} \frac{\partial}{\partial T_m} \left(\frac{\partial T^e}{\partial x} \right) + K_y \frac{\partial T^e}{\partial y} \frac{\partial}{\partial T_m} \left(\frac{\partial T^e}{\partial y} \right) \right.$$

$$\left. + K_z \frac{\partial T^e}{\partial z} \frac{\partial}{\partial T_m} \left(\frac{\partial T^e}{\partial z} \right) - Q \frac{\partial T^e}{\partial T_m} + \lambda \frac{\partial T}{\partial t} \frac{\partial T^e}{\partial T_m} \right] dV$$

$$+ \int_S \left[q \frac{\partial T^e}{\partial T_m} + hT \frac{\partial T^e}{\partial T_m} - h T_\infty \frac{\partial T^e}{\partial T_m} \right] dS$$

Recalling from equation [A-2] that $T = [N] \{T\}^e$ and noting that $\frac{\partial T}{\partial T_m} = [N]$ and substituting this into the functional minimization equation [6], the following is obtained

$$\frac{\partial I(T)}{\partial T_m} = 0 = \int_V \left[K_k \left[\frac{\partial N}{\partial x} \right] \{T\}^e \frac{\partial N_m}{\partial x} + K_y \left[\frac{\partial N}{\partial y} \right] \{T\}^e \frac{\partial N_m}{\partial y} \right.$$

$$\left. + K_z \left[\frac{\partial N}{\partial z} \right] \{T\}^e \frac{\partial N}{\partial z} - Q N_m + \lambda \left[N \right] \frac{\partial T^e}{\partial t} N_m \right] dV \qquad [7]$$

$$+ \int_S \left[q N_m + h \left[N \right] \{T\}^e N_m - h T_\infty N_m \right] dS$$

For all nodes of the element this form of the functional minimization equation can be written in matrix notation as

$$[K] \{T\} + [C] \frac{\partial T}{\partial t} + \{F\} = 0 \qquad [8]$$

where the element contributions are

$$[c^e] = \int_V \lambda [N]^T [N] \, dV \qquad [9]$$

$$[k^e] = \int_V [B]^T [D] [B] \, dV + \int_S h [N]^T [N] dS \qquad [10]$$

$$[f^e] = -\int_V Q [N]^T \, dV + \int_S q [N]^T - hT_\infty [N]^T \, dS \qquad [11]$$

$$[D] = \begin{bmatrix} K_x & 0 & 0 \\ 0 & K_y & 0 \\ 0 & 0 & K_z \end{bmatrix} \qquad [12]$$

$$[B] = \frac{1}{6V} \begin{bmatrix} b_i & b_j & b_k & b_l \\ c_i & c_j & c_k & c_l \\ d_i & d_j & d_k & d_l \end{bmatrix} = \begin{bmatrix} \frac{\partial N_i^e}{\partial x} & \frac{\partial N_j^e}{\partial x} & \frac{\partial N_k^e}{\partial x} & \frac{\partial N_l^e}{\partial x} \\ \frac{\partial N_i^e}{\partial y} & \frac{\partial N_j^e}{\partial y} & \frac{\partial N_k^e}{\partial y} & \frac{\partial N_l^e}{\partial y} \\ \frac{\partial N_i^e}{\partial z} & \frac{\partial N_j^e}{\partial z} & \frac{\partial N_k^e}{\partial z} & \frac{\partial N_l^e}{\partial z} \end{bmatrix}. \qquad [13]$$

V = volume of the element

The terms in the [B] matrix are obtained by calculating the appropriate co-factor of the $[M]^{-1}$ matrix of equation [A-14]. Integration of equation [9] produces the element

capacitance matrix in the form

$$[c^e] = \frac{\lambda V}{20}\begin{bmatrix} 2 & 1 & 1 & 1 \\ 1 & 2 & 1 & 1 \\ 1 & 1 & 2 & 1 \\ 1 & 1 & 1 & 2 \end{bmatrix} \qquad [14]$$

If a finite element is on the surface of the discretized solid, at least three nodes of the tetrahedron will be exposed to the fluid surrounding the solid. These three nodes delineate a triangular area which forms the side of the tetrahedron exposed to the surrounding fluid. When this is the case for nodes j, k, l, the surface integral in equation [10] becomes

$$\int_S h[N]^T[N]dS = \frac{hA_{jkl}}{12}\begin{bmatrix} 0 & 0 & 0 & 0 \\ 0 & 2 & 1 & 1 \\ 0 & 1 & 2 & 1 \\ 0 & 1 & 1 & 2 \end{bmatrix} \qquad [15]$$

A_{jkl} = area of element face formed by nodes j, k, l.

The matrix pattern of equation [15] will vary for other nodal combinations forming the exposed surface area. The

surface integral of equation [11] for nodes j, k, l yields

$$\int_S q \left[N\right]^T - h\, T_\infty \left[N\right]^T dS = \frac{qA_{jkl}}{3} \begin{bmatrix} 0 \\ 1 \\ 1 \\ 1 \end{bmatrix} - \frac{h\, T_\infty\, A_{jkl}}{3} \begin{bmatrix} 0 \\ 1 \\ 1 \\ 1 \end{bmatrix} \qquad [16]$$

When internal heat generation is present, the volume integral of equation [11] takes the form

$$\int_V \left[N\right]^T Q dV = \frac{QV}{4} \begin{bmatrix} 1 \\ 1 \\ 1 \\ 1 \end{bmatrix} \qquad [17]$$

V = volume of the element.

There are several methods for solving the time dependent relationship portrayed by the matrix equation [8]. One such method is to introduce finite elements in time. The limitations of this method are the need for greater computer storage requirements and increased computational effort (Pinder and Gray, 1977). The more commonly used procedure involves a weighted finite difference scheme. This procedure, when used to solve equations like those of

equation [8], appears as

$$[K](\varepsilon\{T\}_{t+\Delta t} + (1 - \varepsilon)\{T\}_t) + \frac{1}{\Delta t}[C](\{T\}_{t+\Delta t} - \{T\}_t) = \qquad [18]$$

$$\varepsilon\{F\}_{t+\Delta t} + (1 - \varepsilon)\{F\}_t$$

t = time

Δt = time increment

The value of ε determines the type of solution that will be obtained. Table 3 summarizes the types of solutions obtained when ε is selected as 0, 1/2, or 1. The neutral stability and second order accuracy make the Crank-Nicholson Central Difference technique appear more attractive than the purely Explicit and Implicit methods. Pinder and Gray (1977) have evaluated finite element, finite difference and lagged finite difference techniques and judged the finite difference method to be, "...the best overall choice in the majority of transient finite element analyses." In this work the Crank-Nicholson Central Finite Difference technique was employed.

Table 3: Summary of Weighted Finite Difference Schemes

	Method Name	Computational Effort	Stability	Accuracy
0	Explicit	Minimal	Conditionally	First order
1/2	Crank-Nicholson Central Difference	More than implicit method	Neutrally	Second order
1	Implicit	More than explicit method	Usually unconditionally	First order

The finite difference representation of the time derivative of temperature at a node evaluated at the midpoint of a time interval is expressed as

$$\frac{dT}{dt} = \frac{T_1 - T_0}{\Delta t} \qquad [19]$$

T = nodal temperature

0 = time t

1 = time at t + Δt

t = incremental change in time

Since the derivative is being evaluated at the midpoint of the time interval, the temperature and force vectors of equation [8] must also be evaluated at that point in time. They can be expressed as

$$\{T\}^* = \frac{\{T\}_1 - \{T\}_0}{2} \qquad [20]$$

$$\{F\}^* = \frac{\{F\}_1 - \{F\}_0}{2} \qquad [21]$$

Substituting equation [20] and equation [21] into equation [8] for {T} and {F} respectively yields

$$[K]\left(\frac{\{T\}_1 - \{T\}_0}{2}\right) + [C]\left(\frac{\{T\}_1 - \{T\}_0}{\Delta t}\right) + \left(\frac{\{F\}_1 - \{F\}_0}{2}\right) = 0 \qquad [22]$$

Multiplying through by 2 and grouping terms based on like temperature vectors produces

$$([K] + \frac{2}{\Delta t}[C])\{T\}_1 + ([K] - \frac{2}{\Delta t}[C])\{T\}_0 + \{F\}_1 - \{F\}_0 = 0 \qquad [23]$$

Rearranging so that only $\{T\}_1$ terms are on the left hand side of the equation gives

$$([K] + \frac{2}{\Delta t}[C])\{T\}_1 = (\frac{2}{\Delta t}[C] - [K])\{T\}_0 + \{F\}_0 - \{F\}_1 \qquad [24]$$

which is of the form

$$[A]\{T\}_{new} = [P]\{T\}_{old} - \{F\} \qquad [25]$$

At time t, the terms on the right hand side of equation [25] are known and a solution must be obtained for $\{T\}_{new}$.

Since that equation is of the form

$$[A]\{T\}_{new} = \{F\}, \qquad [26]$$

it can be solved by standard computer routines designed to solve linear simultaneous equations of this form.

Inclusion of Boundary Conditions

The boundary conditions and assumptions for this problem included 1) specified temperature along the surface of the pond where soil and water were in contact, 2) constant soil temperature at some depth below the pond, 3) no heat flow parallel to the soil surface below the pond bottom and at some distance from the pond and 4) calculated radiation, evaporation and convection fluxes to or from the soil surface. These conditions are clarified by the use of Figure 6. A fifth boundary condition of no heat flux across lines of symmetry, not shown in the figure, allowed the exploitation of symmetry to reduce the size of the domain to be modeled.

Inclusion of these boundary conditions in the computer model required that the appropriate equations be applied to the elements and that these elemental equations be inserted

into the correct positions in the assembled (global) matrices and vectors. In the case of a specified temperature, this was accomplished as described by equation [A-19]. The boundary condition of zero heat flux parallel to the soil surface below the pond and at some distance from the pond was easily accomplished by specifying that the values of the elements in the force vector for those nodes were zero in equation [25]. The boundary conditions which were the most difficult to specify were those which occurred at the soil-atmosphere interface. Where those boundary conditions occured, the element would usually have only one of its triangular surfaces specified by three of its nodes exposed to the atmosphere. The three exposed nodes determined which rows and columns of the element matrix equations would be non-zero (see equations [15] and [16]).

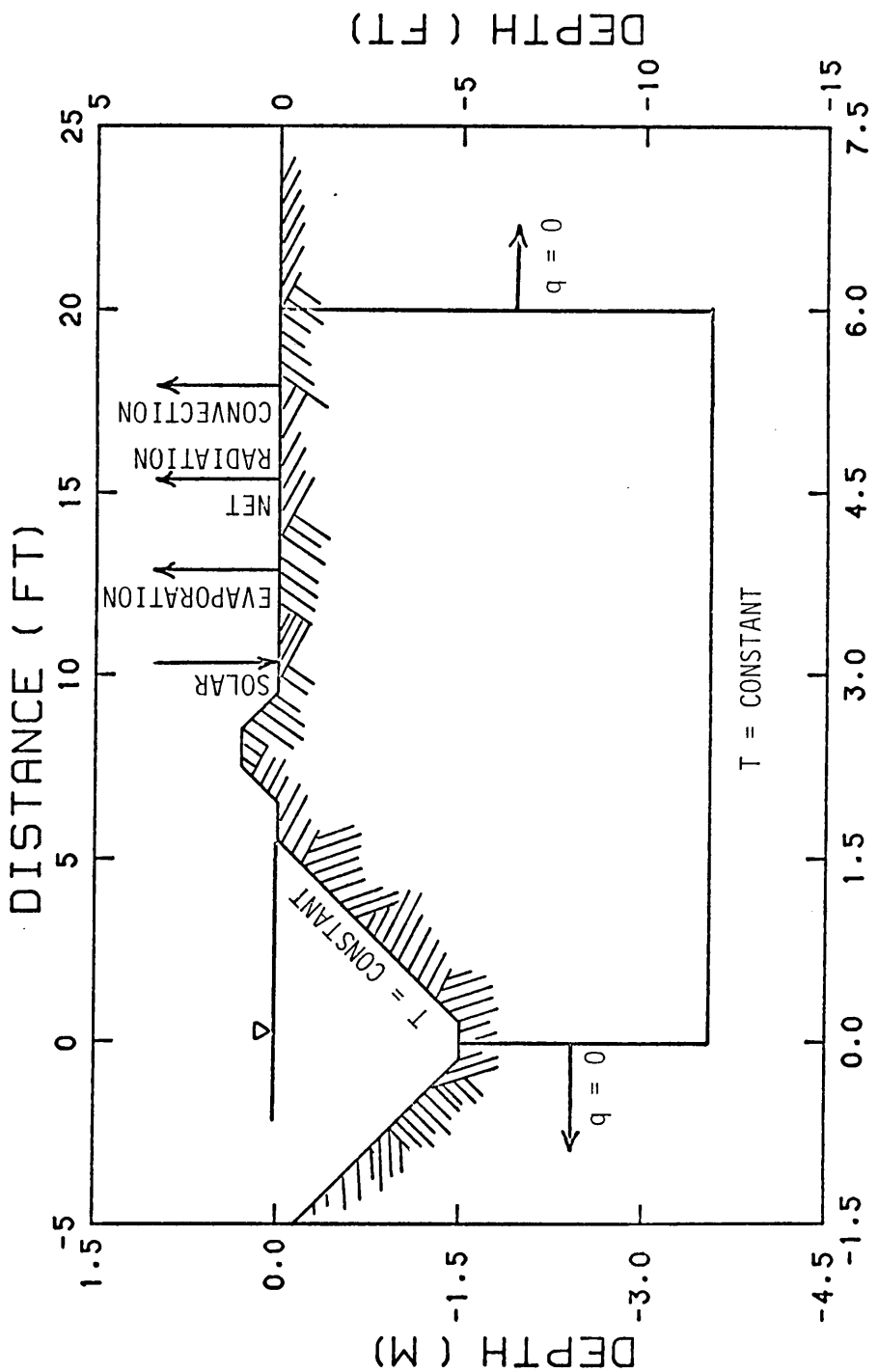

FIGURE 6 BOUNDARY CONDITIONS

Once this was determined for each element, the values of the elemental boundary condition equations could be added into the global matrix equation [25].

The equations discussed thus far have all been linear functions of temperature except for the ones which characterize the radiative energy loss from the soil surface to the sky. This phenomenon obeys the non-linear radiation heat transfer equation that is a function of temperature raised to the fourth power, namely

$$q = \varepsilon \sigma (T_{soil}^4 - T_{sky}^4) \qquad [27]$$

σ = Stefan-Boltzmann constant

T_{soil} = soil temperature (absolute)

T_{sky} = effective sky temperature to which the soil is exposed (absolute)

q = radiation energy flux.

ε = emissivity

Equation [27] may be rearranged into a linear form when the absolute temperature difference is not large. The linear form is written as

$$q = \sigma (T_{soil}^2 + T_{sky}^2)\ (T_{soil} + T_{sky})\ (T_{soil} - T_{sky}) \qquad [28]$$

which is of the form

$$q = h_r(T_{soil} - T_{sky}) \qquad [29]$$

h_r = radiative heat transfer coefficient.

The temperatures used in h_r must be in the absolute scale for the units to match, however those used in the difference can be in degrees Fahrenheit or Celsius depending on which Stefan-Boltzmann constant is used. This makes it convenient when inserting the radiation equation directly into the matrix equations. To allow this linearization to be used without iteration, it was assumed that the energy loss from the soil does not appreciably change the soil surface temperature from one time increment to the next, thereby producing an erroneous radiative heat transfer coefficient. Such an assumption is valid when relatively small time increments are involved and the heat capacity of the soil is sufficiently high.

Convection Model

When the model was originally conceived, convection heat loss calculations were to be made for the soil surface at some distance from the pond as well as in the vicinity of the pond itself. Consequently, a relationship was sought

which would relate heat lost from a relatively flat surface to wind speed and soil and air temperatures. Conventional convection heat transfer coefficient equations employ a characteristic length of the body transferring heat in their formulation. In this problem there was no characteristic length, therefore, that type of formulation could not be applied.

A review of the literature found several relationships for establishing a convection heat transfer coefficient for airflow over large flat surfaces. McAdams established the following relationship based on work he performed with 0.5m (1.64 ft) square vertical copper plates

$$h = 1.09 + 0.23\ V \qquad (V \leq 16) \qquad [30]$$

$$h = 0.53\ V^{0.78} \qquad (16 < V \leq 100) \qquad [31]$$

h = convection heat transfer coefficient (BTU/h-ft^2-^{0}F)

V = air speed (ft/sec)

Since the original work was done, these equations have been modified and appear in the ASHRAE Handbook of Fundamentals (1977) as

$$h = 0.99 + 0.21\ V \qquad (V \leq 16) \qquad [32]$$

$$h = 0.50\ V^{0.8} \qquad (16 < V \leq 100) \qquad [33]$$

Beard and Hollen (1969) used an average of others' results concerning the variation of shear stress with wind speed and found

$$\tau = 28.2 \times 10^{-4}\ \rho V^2/g_c \qquad \text{for rough water} \qquad [34]$$

$$\tau = 19.75 \times 10^{-4}\ \rho V^2/g_c \qquad \text{for smooth water} \qquad [35]$$

τ = surface shear stress

V = air speed

ρ = density of air

g_c = gravitational constant

This value of shear stress was then used in the Reynolds analogy to solve for the convection heat transfer coefficient as

$$h = \frac{g_c \tau}{V}\left[C_p\left(\frac{k}{\mu}\right)^2\right]^{1/3} \qquad [36]$$

C_p = specific heat of air at constant pressure

k = thermal conductivity of air

μ = absolute viscosity of air

Bolz and Tuve (1970) tabulated values of the convective heat transfer coefficient as a function of air speed for a vertical flat plate without verifying the source of the table.

The convection heat transfer coefficient as a function of wind speed is plotted in Figure 7 based on the equations and values proposed by the previously mentioned sources. The equation used by Beard and Hollen (1969) for smooth water is probably not applicable for convection heat loss from the soil and will not be considered further. From Figure 7 it is apparent that the relationships presented by Beard and Hollen (1969) for rough water, by ASHRAE (1977) and by Bolz and Tuve (1970) produce similar results for wind speeds up to 6.1 m/sec (20 ft/sec), but the values of the convection heat transfer coefficients tend to diverge beyond this wind speed. Beyond a wind speed of 6.1 m/sec (20 ft/sec) the extrapolation of the Bolz and Tuve (1970) values and the results of the Beard and Hollen (1969) equation never differ by more than 20% from the values produced using the ASHRAE (1977) equations. For this reason, the pair of ASHRAE (1977) equations were used to model the convection heat transfer coefficient used in equations [15] and [16].

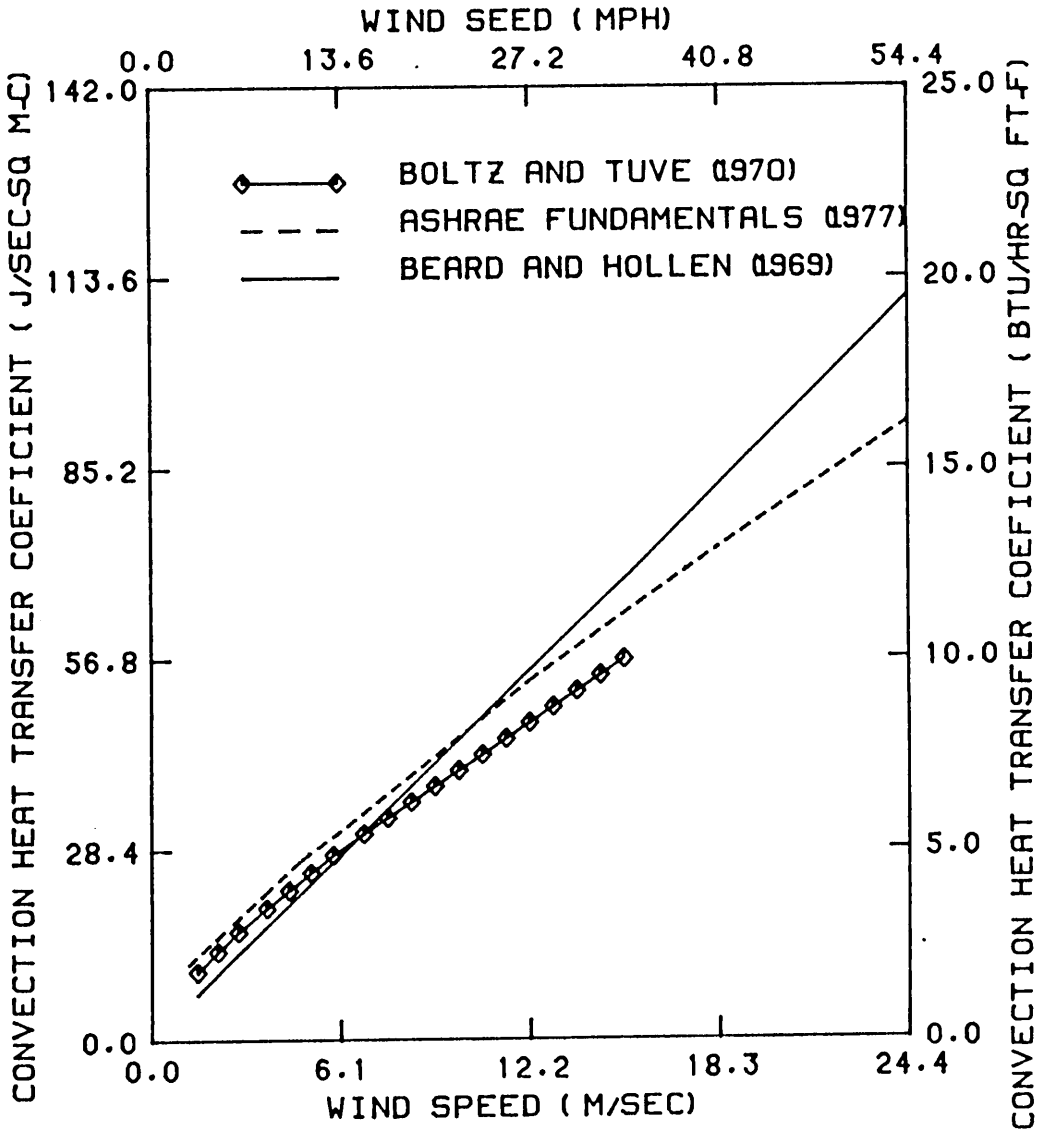

FIGURE 7 CONVECTION HEAT TRANSFER COEFICIENT VS WIND SPEED

Radiation Model

Net long wave radiation from the soil surface to the sky follows the Stefan-Boltzmann Law shown in equation [27]. On a clear night, moisture and carbon dioxide in the atmosphere intercept some of the energy radiated from the surface and reradiate it back to the earth. For this reason, the temperature of the sky to which the soil is radiating can not be considered at absolute zero. Kreith (1965) stated that this temperature is on the order of -45.5 °C (-50 °F) on a cold clear night. Van Wijk (1976) estimated that a body at 7 °C (45 °F) emits long wave radiation as a black body at the rate of 5.229×10^4 J/h-m^2 (110.5 BTU/h-ft^2), while the net radiation from soil has been measured as 24-36% of this value with a clear sky. Sutton (1953) tabulated results produced by various sources which show nocturnal radiation in the range of 22-49% of radiation to a black body for surface temperatures in the range of -8 °C to 30 °C (17.6-86 °F). Sutton (1953) also tabulated results of work done by Simpson (1928) which were an estimate of nocturnal radiation to a clear sky at locations where the vapor pressure of the air was greater than 1 millibar. The results of these sources are summarized in the graph of Figure 8.

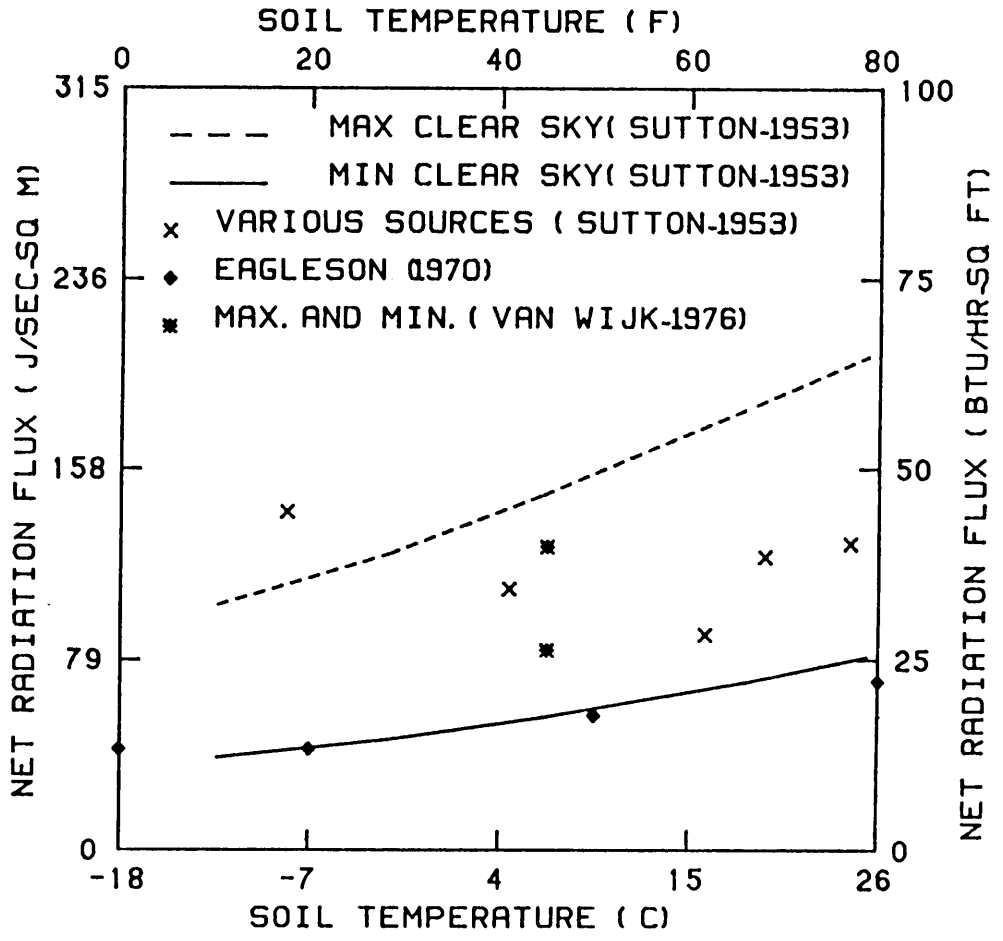

FIGURE 8 NET LONG WAVE RADIATION FLUX VS SOIL TEMPERATURE

Eagleson (1970) presented a graph of radiation intensity using the Stefan-Boltzmann Law for various body temperatures and emissivities, which was first published by the U.S. Army Corps of Engineers. On this graph the emissivity of clear sky had the value of 0.75. Assuming the soil radiated with an emissivity of 0.90, a net radiation (soil radiation - sky reradiation) was obtained and also plotted on Figure 8. It is interesting that these values follow quite closely the minimum curve suggested by Simpson (1928). Other net radiation calculations with the curve presented by Eagleson (1970) did not produce the maximum curve suggested by Simpson (1928).

Van Wijk (1976) suggested a net radiation model that has been proposed by Brunt and also by Angstrom which is of the form

$$H = \varepsilon \sigma (T_{soil})^4 - f(p)(T_{air})^4 \qquad [37]$$

H = net heat loss from soil

ε = emissivity

σ = Stefan-Boltzmann constant

T_{soil} = absolute temperature of the soil

T_{air} = absolute temperature of the air at a short distance (several feet) above the ground.

$f(p)$ = empirical function of the square root of partial pressure of moisture in the air.

Brunt and Angstrom each had a different formulation for the function f(p), but the major limitation for using the function is that the coefficients of the function must be determined for each locality. The magnitude of these coefficients also vary substantially from one locality to the next. Thus, it is difficult to generalize the equation outside of the region for which the coefficients are known. The presence of a coefficient on the $(T_{air})^4$ term does not allow linearization of the equation as discussed in the Inclusion of Boundary Conditions section. Consequently, this type of model was not pursued.

Various sources contributed to forming the model that was finally developed. Van Wijk (1976) suggested that the net radiational heat loss should be multiplied by a factor to account for cloud cover. This factor takes the form

$$\text{factor} = 1 - mv \qquad [38]$$

m = cloud cover (tenths)

v = cloud type factor

v = 0.9 low clouds

v = 0.2 cirrus clouds

v = 0.8 average

Kreith (1965) suggested that the emissivity to be used

when two gray bodies are exchanging radiation can be calculated by the formula

$$\varepsilon_{net} = \frac{1}{\left(\frac{1}{\varepsilon_1} + \frac{1}{\varepsilon_2} - 1\right)} \qquad [39]$$

When ε_{soil} is equal to 0.91 and $\varepsilon_{clear\ sky}$ is equal to 0.75, the value of ε_{net} is 0.7.

Brunt's and Angstrom's function f(p) did not increase in value for increases in the partial pressure of moisture in air beyond about 3123.3 Pa (0.453 psi). In the model, a function called VAPFAC was developed which had the value of zero at a partial pressure of zero and increased linearly to the value of one at a partial pressure of 3123.3 Pa (0.453 psi). The value of VAPFAC then remained constant at the value of one for larger values of partial pressure.

With this information available, the radiation model was developed as

$$H = \varepsilon_{net}\ \sigma\ coef\ [(T_{soil})^4 - (T_{clear\ sky})^4] \qquad [40]$$

$$coef = [1 - A*VAPFAC(1-VAPFAC/2) - m * v] \qquad [41]$$

A = constant

Testing of the model showed that Simpson's upper and lower limits of clear sky radiation could be modeled with best results (see Figure 9) when the following values were assumed in this set of equations:

Upper limit:

VAPFAC	= 0.0
v	= 0.0
Tclear sky[1]	= 400 R
ε_{net}	= 0.7
A	= 1.25

Lower Limit:

VAPFAC	= 1.0
v	= 0.0
Tclear sky[1]	= 400 R
ε_{net}	= 0.7
A	= 1.25

Increases in the cloud cover factor (m) produced appreciable reductions in the net radiation heat loss even with low values of VAPFAC. When the value of VAPFAC was greater than 0.175 and cloud cover factor (m) was equal to 1.0, the value of (coef) became negative.

---

[1] (Kreith, 1965, had suggested approximately 410 R.)

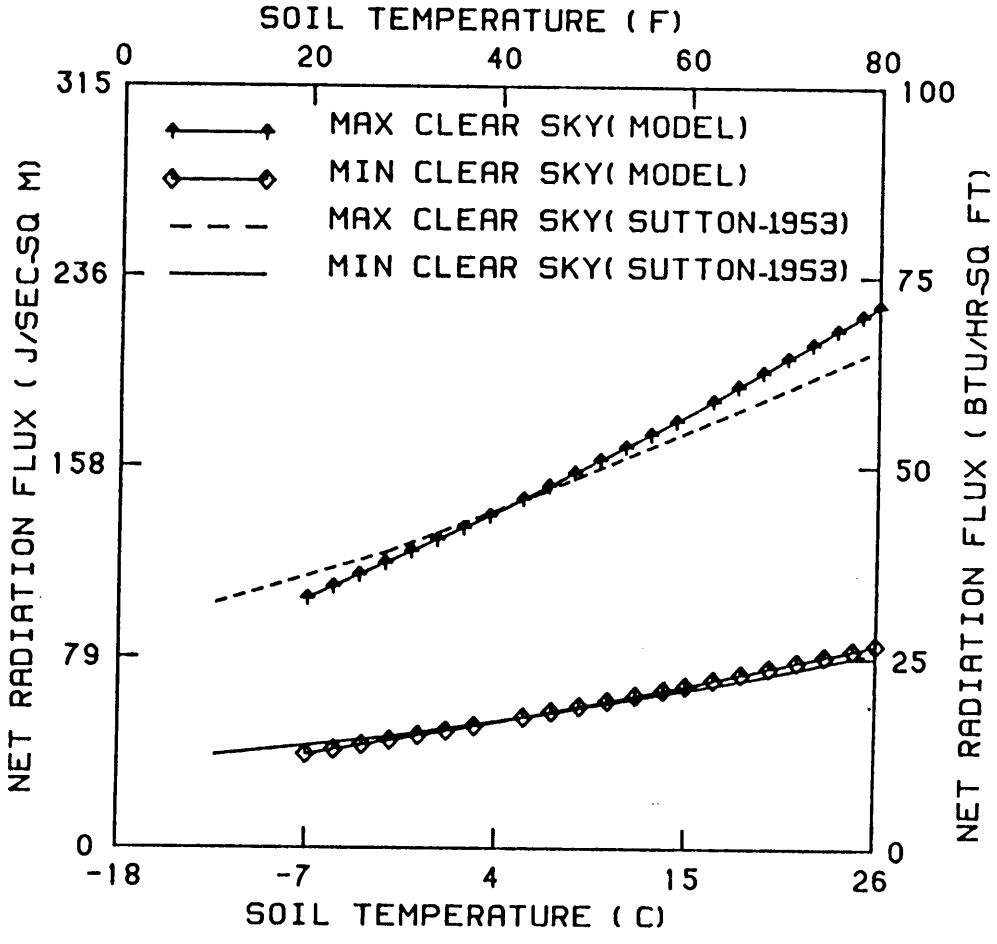

FIGURE 9 NET LONG WAVE RADIATION FLUX VS SOIL TEMPERATURE

A check in the computer program sets the variable (coef) equal to a small value greater than zero when this occurred. The partial pressure of 120.7 Pa (0.07^{0} psi) produced a VAPFAC equal to 0.175. This would be considered a moderate to high air moisture condition for temperatures between about -1 ^{o}C (30 ^{o}F) and 4 ^{o}C (40 ^{o}F). Below -1 ^{o}C (30 ^{o}F) this vapor pressure could not exist. Therefore, the prediction of low net radiation from the soil under high moisture air and full cloud cover is not unreasonable.

Solar Radiation Model

Solar radiation on the soil surface is an energy input to that boundary. Consequently, a model was developed which used measured solar radiation incident on a south facing surface sloped at an angle of 52 degrees from the horizontal. The model was based on equations provided by Duffie and Beckman (1974). Input variables include

1. solar radiation incident on a south facing surface elevated 52 degrees from horizontal,
2. number of the day of the year,
3. value for the equation of time provided in a graph (Figure 2.7.1, page 19, Duffie and Beckman, 1974),
4. hour of day,
5. absorptivity of the soil surface, and
6. data characteristic of the location (Blacksburg, VA)

are constants in the model and must be changed for different locations.

The model had the capability of calculating the solar flux incident on a horizontal surface and on surfaces facing south, east, and west sloped at 45 degrees. The radiation calculated as incident on the sloped surfaces was to be applied to the pond berm surfaces. Since these surfaces were not included in the boundary of the problem to be solved (see section on Simplifying Assumptions), no use was made of the values calculated for these sloped surfaces.

Evaporation Model

Evaporation of moisture from the soil surface is another path of energy loss from the soil surrounding the pond. A review of the hydrology and meteorology literature for evaporation models revealed several methods that have been investigated. One model relied on knowledge of air velocity and saturation vapor pressure gradients from the soil surface to some distance above the surface. Mather (1974) described this type of data as being very difficult to obtain with accuracy therefore, it was not collected during this investigation. Other models are more empirical, usually assuming solar energy is the only source of energy available to evaporate water. Since these techniques were not applicable in the situation under consideration, an

attempt was made to estimate the energy losses from the soil surface due to evaporation. During the period that the four electrically heated ponds were being tested, water had to be replaced in ponds that did not have insulation at the water-air interface. The quantity of water added to each pond was measured with a conventional household water meter. The calculated evaporation rate from the ponds was probably the closest estimate of potential evaporation from a free water surface that could be obtained under the conditions of the tests. However, this rate was only the average evaporation rate for the several days between water additions and was for the water surface only. Consequently, a model was sought which might relate evaporation rate from a soil surface to the controlling parameters of soil moisture content at the surface, wind velocity, soil temperature, relative humidity of the air, and average potential evaporation for a period. Such a relationship was developed which incorporated the following expectations:

1) When the soil surface moisture content is at or above field capacity, and the soil temperature is equal to that of the pond water, and the wind speed and relative humidity of the air is equal to the average during which the potential evaporation rate was determined, then the

evaporation rate from the soil should equal the average rate from the pond surface.

2) No evaporation will occur when the surface soil moisture is less than or equal to the wilting point of the soil.

3) Decreasing the soil temperature below that of the pond water temperature will tend to reduce the rate of evaporation until the soil surface freezes, whereupon evaporation from the surface ceases.

4) Air of 100 percent relative humidity has zero potential for promoting evaporation from the soil surface.

5) Decreases in wind speed below the average for the period will produce a linear reduction in the soil evaporation rate. Increases in wind speed will produce the opposite effect.

Based on these observations, the following relationship was developed

$$EVAP = CANCEL*SMOISTF*((WINDF + RELHUMF + STEMPF)/3.0)*PE \quad [42]$$

EVAP = EVAPoration rate from soil.

PE = Potential Evaporation rate; evaporation rate from the pond.

CANCEL = has the value 1, except it is zero when soil temperature falls below 0 ^{o}C (32 ^{o}F).

SMOISTF = Soil MOISTure Factor. Varies linearly from zero at wilt point to one at field capacity. Has the value of one for soil moisture greater than field capacity.

WINDF = WIND speed Factor. Varies linearly from zero at zero wind speed to one at average wind speed for the period. It will have a value greater than one for wind speeds greater than the average.

STEMPF = Soil TEMPerature Factor. Varies linearly from zero at 0 °C (32 °F) to one at 20 C(68 °F).

RELHUMF = RELative HUMidity Factor. Varies linearly and was inversely proportional to ambient air relative humidity. Has the value of one at the average relative humidity for the period and zero at 100 percent relative humidity.

Simplifying Assumptions

It was explain in the Inclusion of Boundary Conditions section that the boundary condition of zero heat flux in the direction away from the pond was assumed at some distance from the pond where isothermal lines in the soil were parallel to the soil surface. During the discretization process it became apparent that modeling such a distance from the pond would produce an excessive number of nodes which would cause computer storage capacity to be exceeded. Several alternatives to this problem were explored. One alternative was off-line storage of data that would normally be stored in computer core memory in the form of subscripted

variables. When these variables are changed frequently, large expenditures for writing to and reading from off-line computer storage devices can be expected. Consequently, this procedure was employed only with those arrays that were not expected to change frequently. Another alternative that also conserved computer core memory was the multiple use of subscripted variable names, that is, when an array was no longer needed for storing one type of information, it was used to store another type, thus avoiding the use of core memory for unneeded information.

Another alternative resulted in some savings in computer core memory storage. Square global matrices with zeroes outside of the banded region were stored as vectors containing the elements of the banded portion of the matrix only, thus eliminating the need for storing the large numbers of zeroes. None of these computer techniques reduced the number of nodes being modeled and, consequently, did not reduce the storage requirements sufficiently. A fourth alternative involved restructuring the model. Since modeling soil temperatures at a large distance from the pond required an excessive number of nodes, an alternative was needed which would require fewer nodes. Upon examination of soil temperature data collected with the buried thermocouples, it became apparent that the soil temperature,

measured at a short distance from the pond edge and at an appropriate depth, did not change very rapidly and could be considered constant for relatively short periods of time (24-48 hours). Figure 10 is a plot of soil temperature versus time for various depths which shows that soil temperatures below about 0.6 m (2 ft) do not change rapidly. For this reason it was concluded that, when modeling over the short term, the boundary of the region could be assumed at a closer distance from the pond if the boundary temperatures below a certain depth were specified and unchanging (see Figure 11). Above the 0.6 m (2 ft) depth, the soil temperature is influenced by variations occurring at the soil-atmosphere interface. This depth is confirmed by Sutton (1953), who claims that diurnal variations in soil temperature are negligible below 0.5-0.6 m (1.8-2.0 ft).

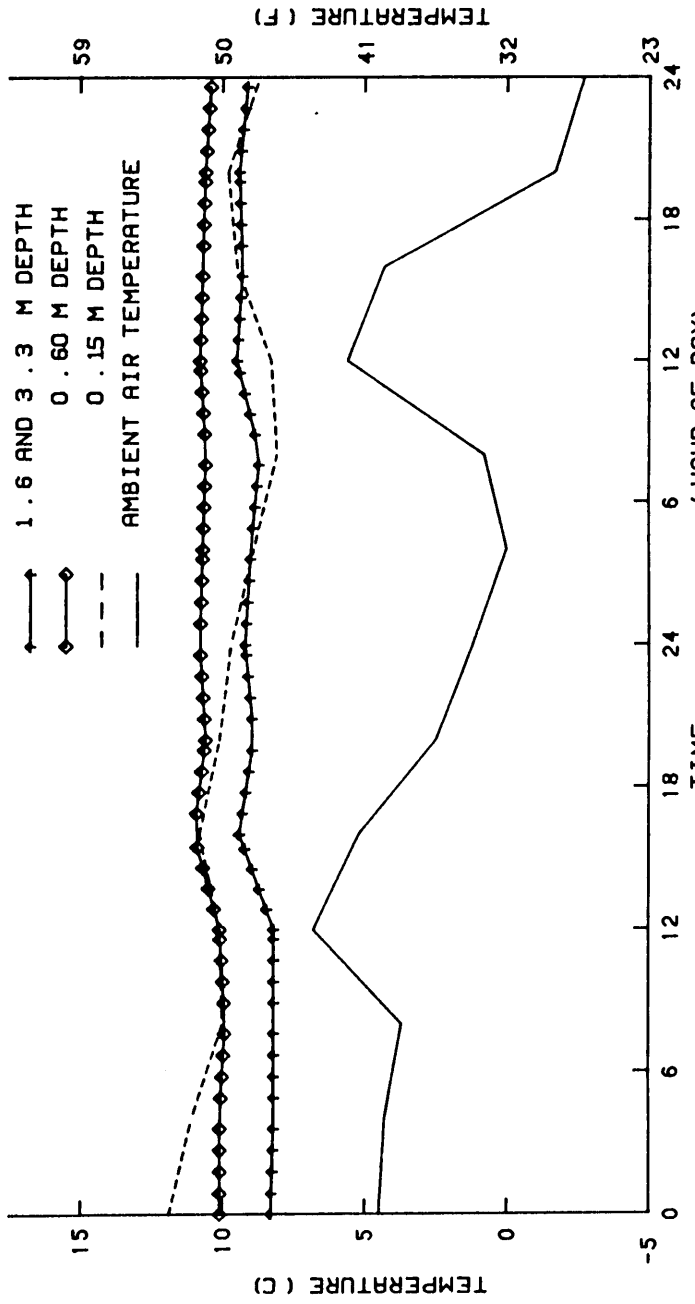

FIGURE 10 SOIL[1] AND AIR TEMPERATURE VS TIME OF DAY
MARCH 16 AND 17, 1978

[1]SOIL TEMPERATURE 0.33 M FROM POND RIM AND ON A LINE PERPENDICULAR TO POND SIDE.

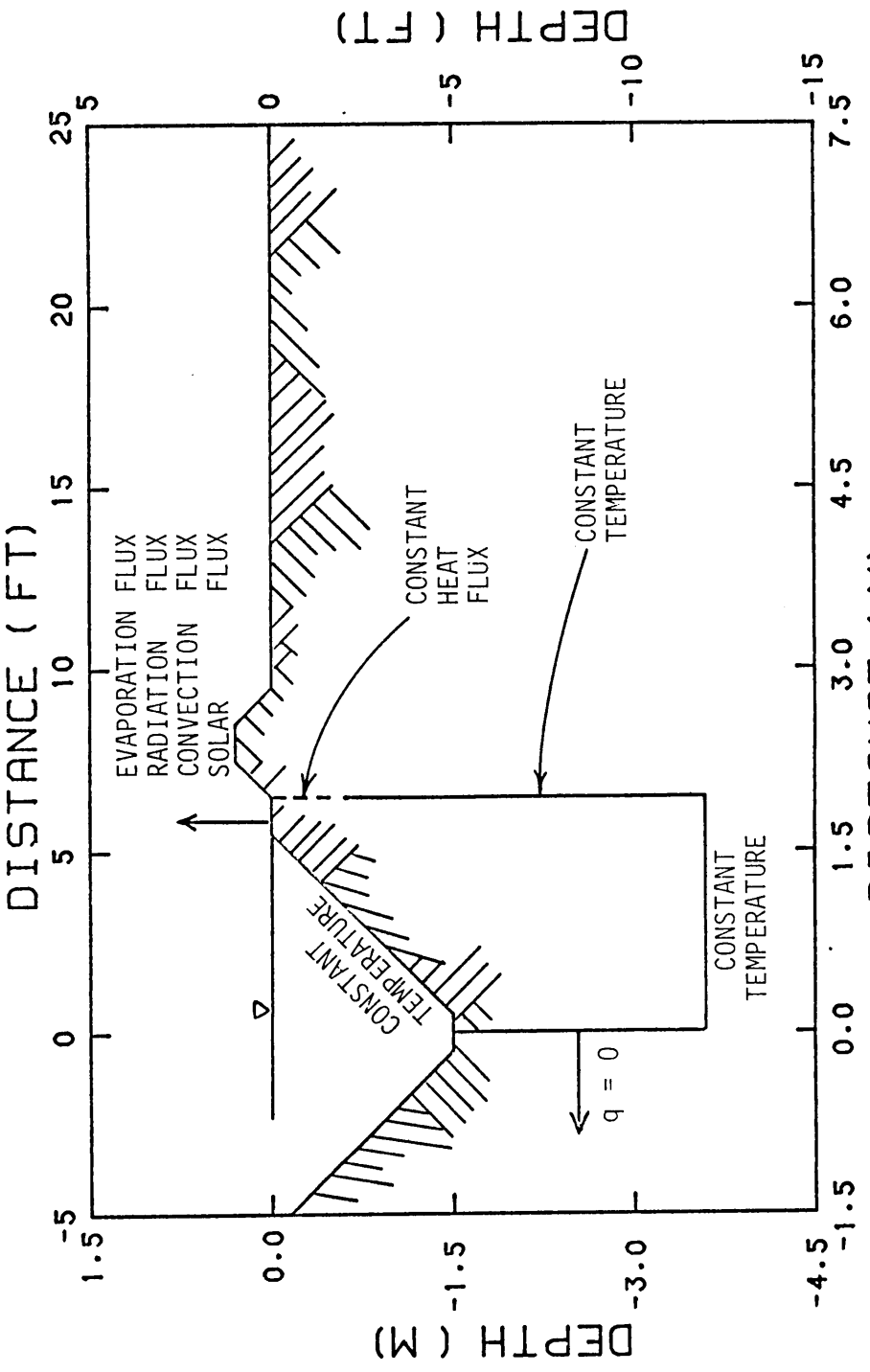

FIGURE 11 BOUNDARY CONDITIONS

Along the boundary and to the depth of the diurnal temperature variations, the boundary condition is estimated as a heat loss through the soil which is a function of an average temperature gradient that might be expected during the period of test. Since energy losses at the soil-atmosphere interface are so large (25 times greater) relative to that lost from a surface node to other soil nodes, errors introduced by this technique for a surface node were insignificant. Errors introduced for a subsurface node are in direct proportion to the error in estimating the gradient. If the soil surface was horizontal (no berm present), the gradient would remain fairly constant even with the nodal temperatures near the surface fluctuating in response to forces occurring in the surroundings. The presence of a berm adds a damping condition for nodes just outside the model boundary which makes it difficult to estimate the gradient. This damping effect may produce a heat flow from the boundary node that is estimated to be a maximum of 50% different from that produced by a constant gradient. Consequently, a gradient for boundary nodes between the ground surface and 0.6 m (2 ft) depth were estimated at the beginning of each test period and this gradient remained constant during the test period. It must be emphasized that this technique is valid only for short

periods of testing and relies quite heavily upon having sufficient data available which places a great restriction on the universality of the model. However, it was necessary that a set of boundary conditions be specified at a short distance from the pond edge so the model could be employed.

After each iteration, the finite element scheme establishes the temperature at each node. Once the temperature distribution is known, the heat flow from the pond can be calculated as the heat flow from a pond surface node to nodes in the soil surrounding the pond. The nodal heat flow calculation scheme was that used by Kreith (1965) as a relaxation technique. This technique is reasonably accurate in the interior of a heat conducting material but is of limited value near the boundaries. In this study, one such location where these limitations occurred was along the top edge of the pond. Here the temperature at the soil-atmosphere interface varied over quite a large range, while that at some depth below the surface of the ground was appreciably damped out. However, the heat flow calculation technique used the temperature of the surface node which may not be representative of the temperature of the region to which heat was flowing. A refinement of the element grid would minimize this problem, although such a refinement would increase computer storage requirements and increase

the time required to obtain each solution.

As water is frozen in the soil, the latent heat of fusion is given up to the air. When this heat of fusion is liberated at the soil surface, it has a tendency to keep the soil temperature closer to that of the freezing point than if no moisture were present to be frozen. In other words, soil moisture freezing damps the low soil surface temperature extremes at the soil-atmosphere interface. Since the elements selected in this study were fairly large and since soil freezing has to be considered on an element by element basis, the latent heat of fusion was not modeled in this study. This may result in lower soil surface temperatures with resultant excess conduction heat loss predictions at the soil surface as discussed in the previous paragraph.

Soil Conductivity

The movement of energy through soil is a complex process. Energy moves through the mineral particles by conduction. This process is limited by particle to particle contact area and the conductivity of the soil minerals. Since the conductivity of water is 22 times greater than that of air, the conductivity in sands increases rapidly as the liquid moisture content of the soil increases, whereas in clays there is a typical lag in soil conductivity as the moisture content increases whereupon it increases suddenly (Figure 12). The explanation for this appears to derive from the larger number of particle-to-particle contact points in a clay compared to a sandy soil and the larger surface area of clay particles compared to sand grains. The larger surface area of the particles in a clay will absorb more water than will the sand. Therefore, much more water must be added to a clay before a water "bridge" forms at the particle contact points. Liquid water accumulates at particle to particle contact points increasing the effective area of contact. This allows energy to flow more easily from one particle to the next (Kohnke, 1968), (Chudnovskii, 1962), (Ioffe and Revut, 1966).

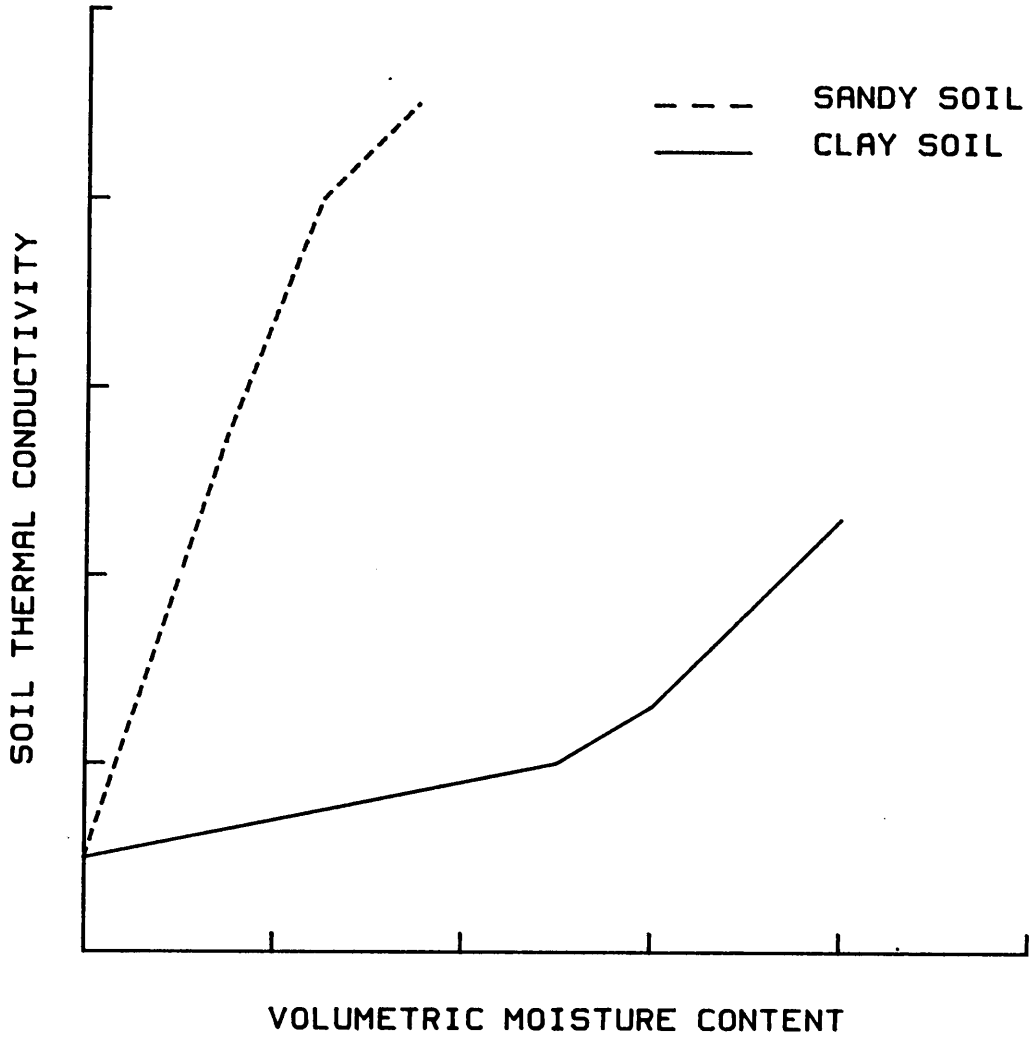

FIGURE 12 SOIL THERMAL CONDUCTIVITY AS A FUNCTION OF VOLUMETRIC MOISTURE CONTENT

As the moisture content increases, soil particles become enclosed in a film of water which provides an easier path for the energy to follow than does the air in the voids. When the soil is saturated, its maximum thermal conductivity is achieved. The maximum thermal conductivity will never equal that of the soil minerals because the water has a thermal conductivity that is only 0.14 that of the soil minerals (Kohnke, 1968). Because clay soils usually have a greater porosity than sandy soils and consequently a lower density of mineral material, the conductivity of clays will be lower than that of sands.

Energy can be transferred in a moist porous medium (i.e. low water content soil) by the process of moisture diffusion. According to Tye (1969), this process can account for relatively large rates of energy transfer in the soil when the soil temperature is above 30 °C (86 °F). Energy transfer between soil particles by radiation can be a significant mode if the soil has large pore size, is at low moisture content and relatively high temperature gradients exist (Ioffe and Revut, 1966). This condition might be encountered in desert soils. Convection heat transfer by the movement of air within the voids of a soil appears to be more significant when the pore size is larger (sands) than when it is smaller (clays) (Ioffe and Revut, 1966). It is

also limited to the case of relatively low soil moisture. Finally, energy transferred by the percolation of excess soil moisture can be the major mode of energy movement in the soil when conditions are conducive for this process.

When this model was conceived, the design temperatures to be expected from the energy storage device were to be in the vicinity of 20 °C (68 °F) and temperature gradients in the soil were expected to be small to moderate. The soil was known to be a clay with small particle size. For these reasons, the effective soil conductivity was expected to be uneffected by the radiation and diffusion modes of heat transfer. Over the period of a winter, the soil moisture content might be expected to remain relatively constant because the presence of frost in the top layers of soil acts as a barrier to water infiltration. The soil moisture should be near the field capacity most of the winter (Amos, 1979). For these reasons the estimates of soil conductivity were based on a soil moisture content of about 32% by volume (Yong and Warkentin, 1966). The computer program has the capacity of accepting any soil conductivity specified for frozen and unfrozen soil. Based on average soil temperature for an element, the program determines which elements are assigned conductivity for frozen soil and which elements are assigned conductivity for unfrozen soil.

As previously mentioned, the model was capable of accepting specified soil thermal conductivity, heat capacity, density, and other pertinent characteristics. Discussions with Amos (1979) established that the soil surrounding the test ponds had an average porosity of 40% and a dry density of 1.5 g/cc (93.6 lbs/ft^3). Assuming field capacity as 32% volumetric moisture content (Yong and Warkentin, 1966), the moist density was calculated to be 1.82 g/cc (113.6 lbs/ft^3). With this information, various sources were consulted to establish soil thermal conductivity and heat capacity. Yong and Warkentin (1966) suggested equation [43] as a means of calculating soil thermal conductivity.

$$k = f_w k_w + f_s k_s \qquad [43]$$

k = thermal conductivity

f = fractional portion of material in the soil

w = refers to soil water

s = refers to soil minerals

They also presented a graph of soil thermal conductivity vs. moisture content (dry weight basis) for a variety of dry densities and soil types. In his thesis, Vaughan (1972)

reported equation [44] for calculating thermal conductivity.

$$k = (0.9 \log M - 0.2)\, 10^{0.01 \lambda_d} \qquad [44]$$

k = thermal conductivity (BTU-in/h-ft^2-^{0}F)

M = moisture content , dry weight basis

λ_d = dry density (lbs/ft^3)

Ioffe and Revut (1966) presented a nomograph from which soil thermal conductivity and heat capacity can be selected. Van Wijk (1976) tabulated some values of soil thermal conductivity as a function of moisture content. These thermal conductivity values and those just mentioned are presented in Figure 13. From this figure, it is apparent that soil conductivity can be quite variable. The soil thermal conductivity was selected as 1.12 J/sec-m-^{0}C (0.65 BTU/h-ft-^{0}F).

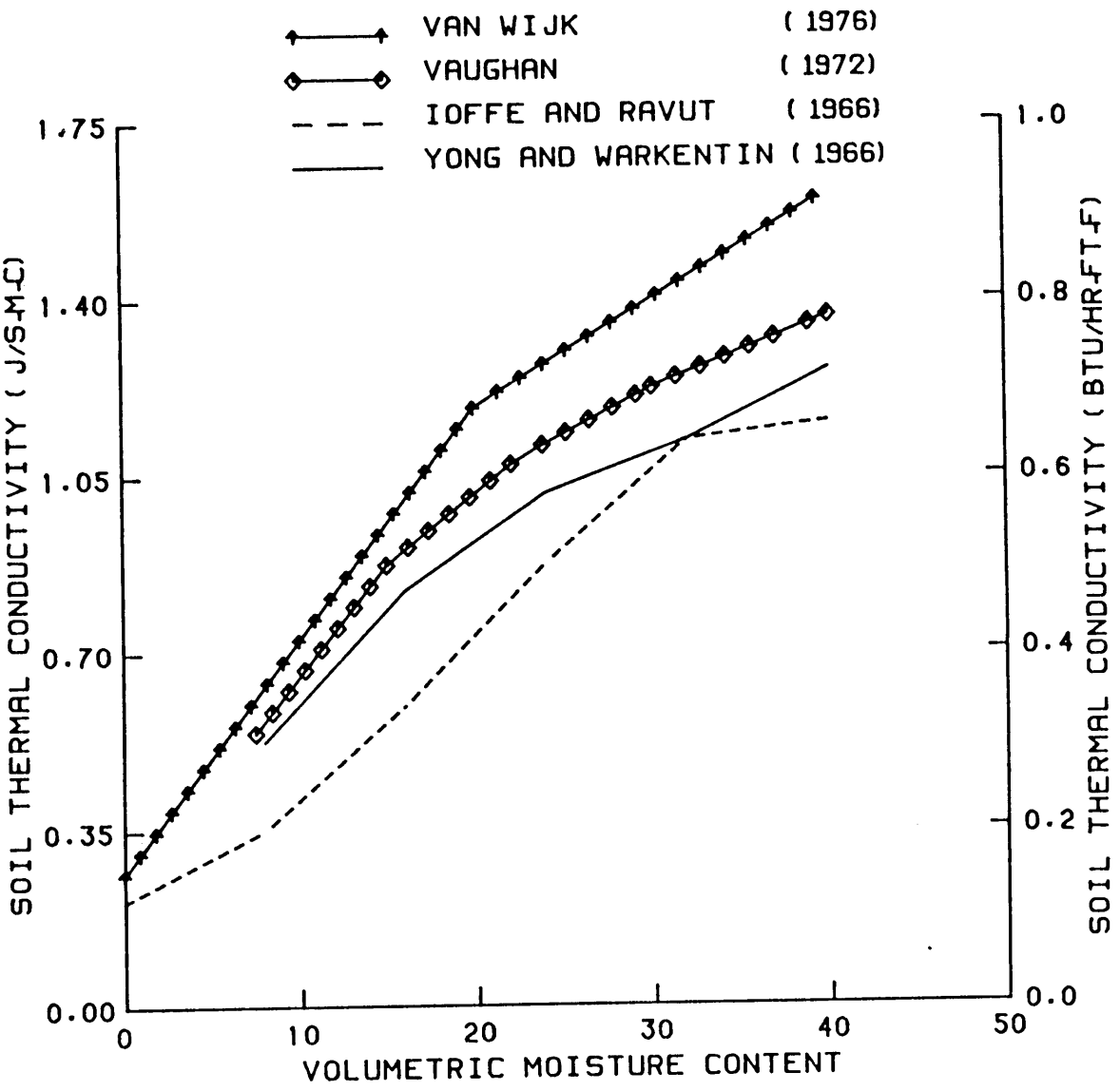

FIGURE 13 SOIL THERMAL CONDUCTIVITY AS A FUNCTION OF VOLUMETRIC MOISTURE CONTENT

The heat capacity of the soil was calculated by equation [45] suggested by Yong and Warkentin (1966).

$$C = \gamma_d C_{sp} + \frac{w}{100} C_w \qquad [45]$$

w = moisture content (dry wt. basis)

C = soil heat capacity

C_{sp} = heat capacity of soil particles

C_w = heat capacity of water

γ_d = soil dry density

The previous assumptions were the basis for calculating the soil heat capacity as 2.507 J/g-^{0}C (0.6 BTU/lb-^{0}F).

RESULTS AND DISCUSSION

Model Verification

To verify the capability of the model, computer Program 4 was executed using measured and interpolated soil temperatures in the vicinity of the pond as initial input data. Weather data were used as input to the model for computing pond heat loss through time.

The initial soil temperature distribution in the vicinity of the pond was obtained by executing Program 2 with temperatures measured at midnight on March 14, 1978. Program 4 was executed with one hour time steps through the period March 15 to March 18, 1978, using solar energy and air temperature data measured at the VPI & SU Swine Center, Blacksburg, relative humidity data measured at the Agricultural Engineering Farm, Blacksburg and average wind speed and cloudiness data measured at Woodrum Field, Roanoke. The weather during the period ranged from cloudy to sunny with average wind speeds reaching a maximum of 9.25 m/sec (20.7 MPH). Ambient air temperatures for the period are plotted in Figures 14 through 17.

To determine how closely the simulated temperatures produced by Program 4 compared with those measured, several

graphs of temperature were plotted. Figures 14 and 15 depict ambient air temperature and soil temperature measured 0.33 m (1 foot) from the pond edge at the 0.15 m (0.5 ft) and 0.66 m(2 ft) depths during the March 15-18, 1978 period. Minimal diurnal variations in temperature exist at the 0.66 m (2 ft) depth. Temperature variations at the 0.15 m (0.5 ft) depth are greater than at the 0.66 m (2 ft) depth. The temperature curve at the 0.15 m (0.5 ft) depth has a similar shape to the ambient air temperature curve, but its maximums and minimums lag behind the maximums and minimums of the ambient air temperature.

Figures 16 and 17 represent ambient air temperature and simulated soil temperatures at the ground surface, 0.33 m (1 ft) and 0.66 m (2 ft) depths. Temperature measured at the 0.15 m (0.5 ft) depth are also plotted in the figures. As shown in these figures, the model predicts soil surface temperature following ambient air temperature quite closely during the days when the sun is shining. On March 15, 1978 solar energy was greatly reduced due to heavy cloud cover.

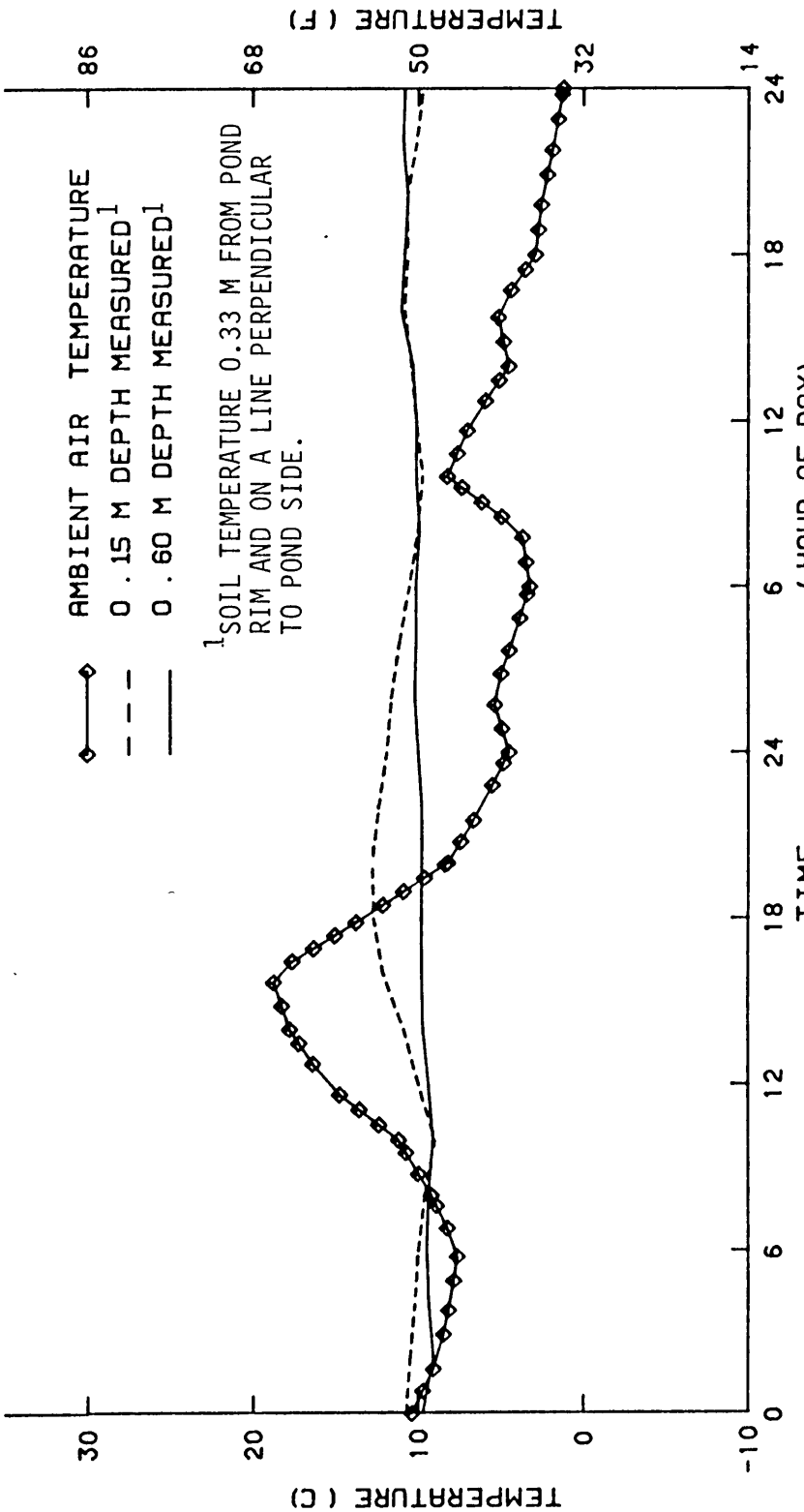

FIGURE 14 SOIL AND AIR TEMPERATURE VS TIME OF DAY
MARCH 15 AND 16, 1978

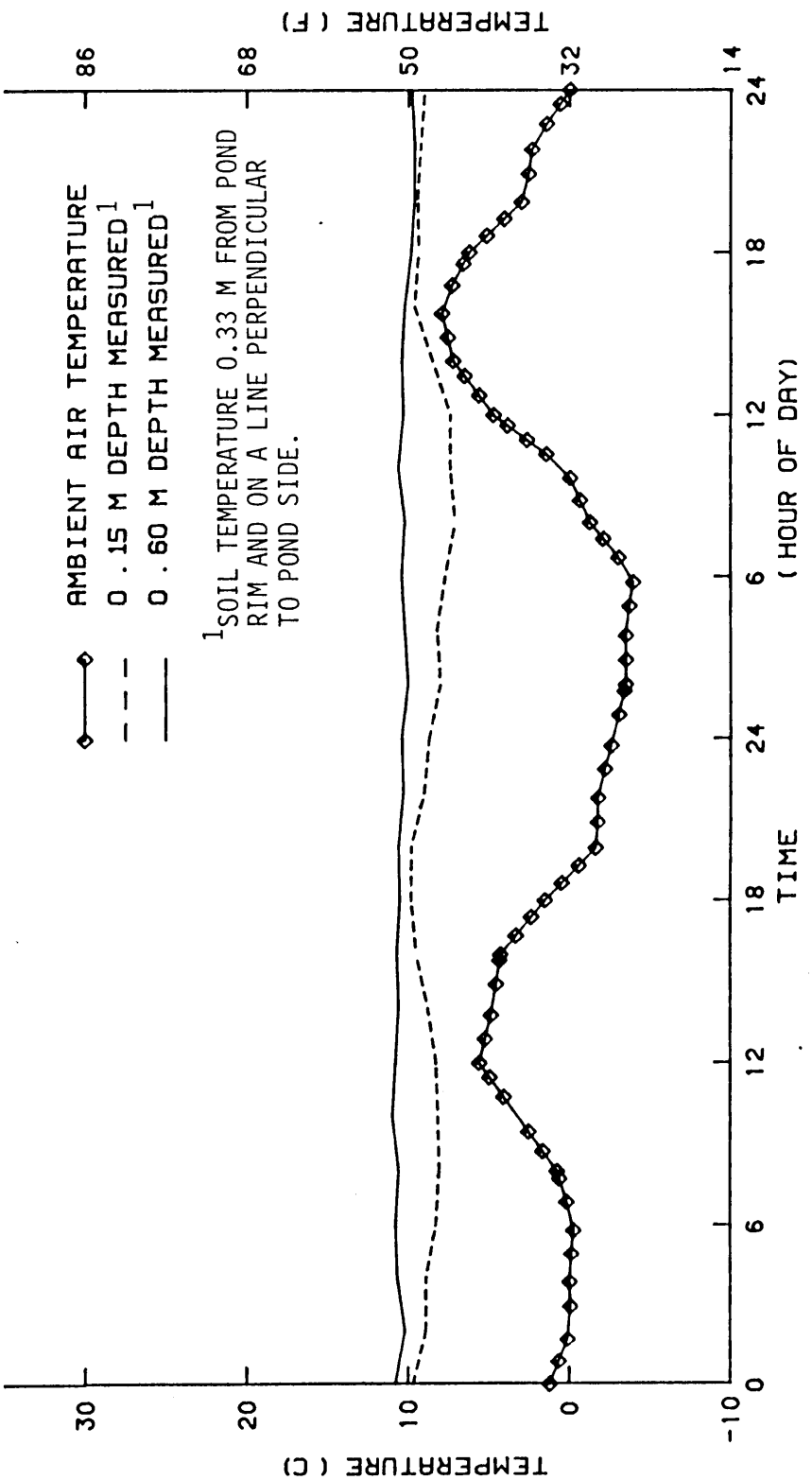

FIGURE 15 SOIL AND AIR TEMPERATURE VS TIME OF DAY
MARCH 17 AND 18, 1978

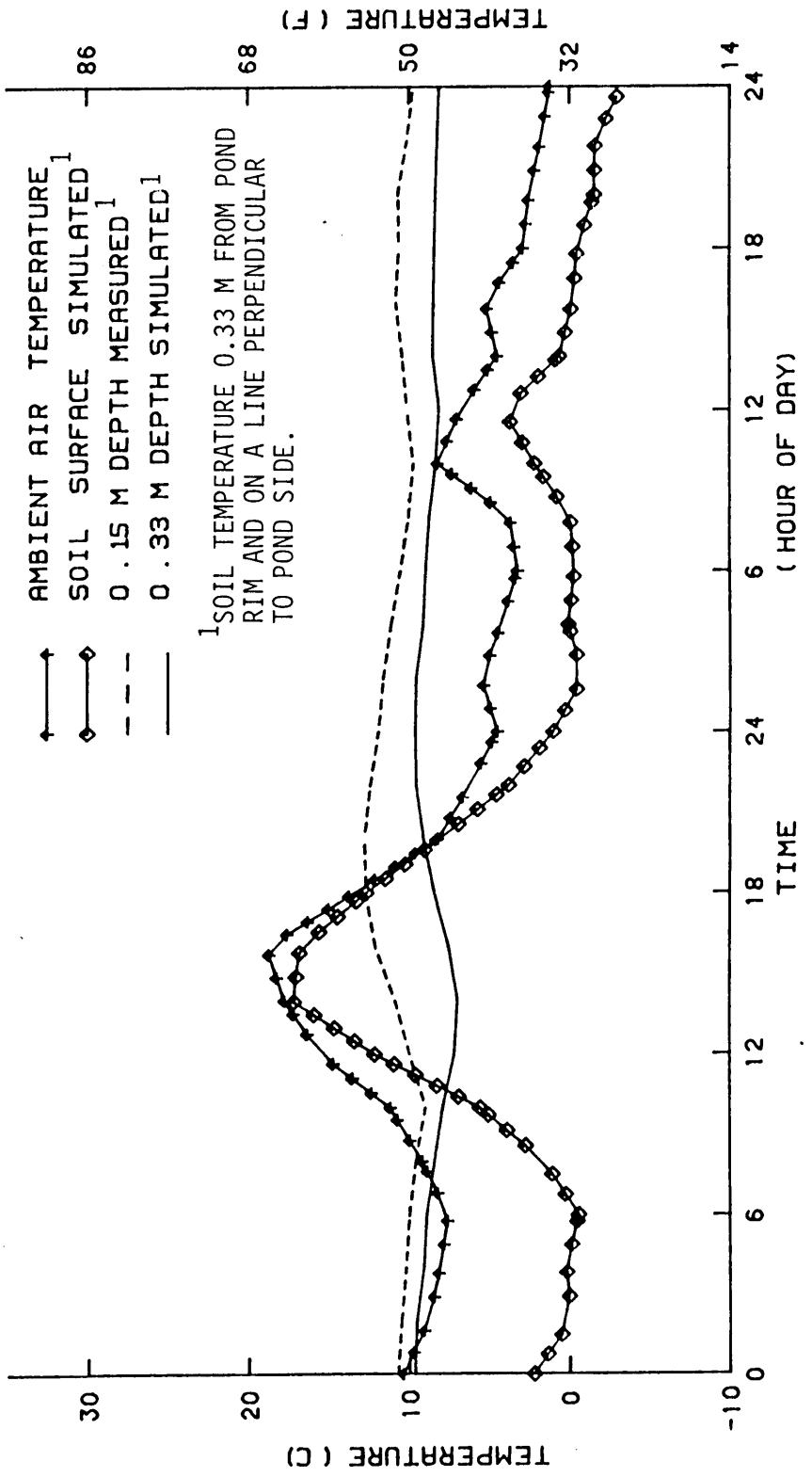

FIGURE 16 SOIL AND AIR TEMPERATURE VS TIME OF DAY MARCH 15 AND 16, 1978

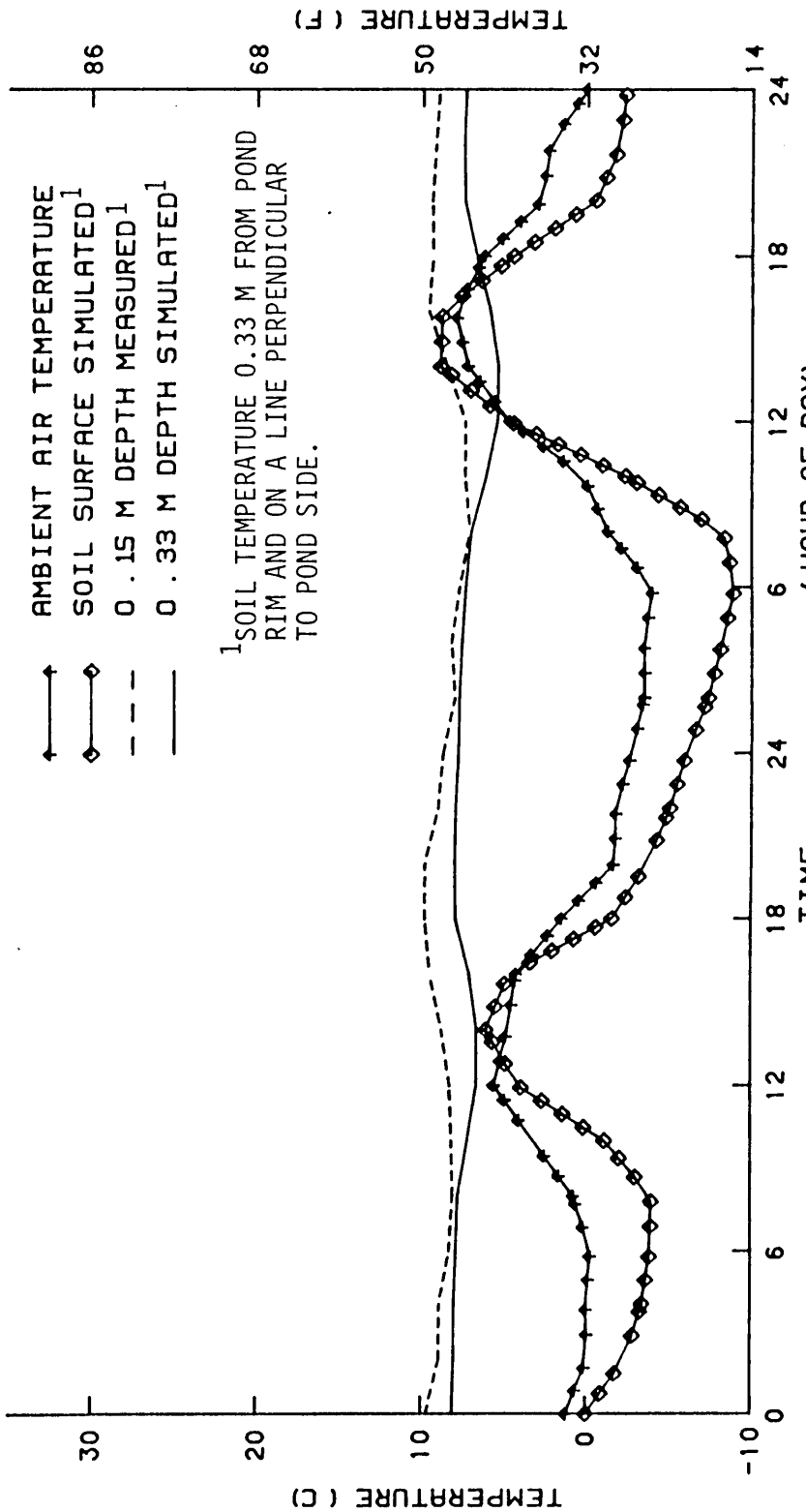

FIGURE 17 SOIL AND AIR TEMPERATURE VS TIME OF DAY MARCH 17 AND 18, 1978

As a result, predicted soil surface temperatures were not so close to the ambient air temperature. Soil surface temperature at night was simulated to be appreciably lower than ambient air temperature, illustrating the effect commonly referred to as radiational cooling and was an example of what can happen when the heat of fusion was omitted from the model as was discussed in the Simplifying Assumptions section. The simulated temperature at the 0.33 m (1 ft) depth increased and decreased over a larger range than did the simulated values at the 0.66 m (2 ft) depth. The simulated maximum and minimum values of temperature at 0.33 m (1 ft) lagged behind those measured at the 0.15 m (0.5 ft) depth. Tables 4 and 5 are a tabulation of the best estimate of the time of occurrence of the maximum and minimum temperature for the various depths. A dash in the table represents the inability to locate a maximum or minimum in the data. Linear regressions were developed for these values and are plotted in Figure 18. It is apparent from this plot and Tables 4 and 5 that the simulated maxima and minima for the various depths occur at the correct time of day compared to the measured values, even though soil temperatures were not measured at either the soil surface or the 0.33 m (1 ft) depth.

Table 4: Time of Maximum Temperature as a Function of Depth

	DEPTH				
	Surface	0.15 m (0.5 foot)	0.33 m (1 foot)	0.66 m (2 foot)	
Date	Simulated	Measured	Simulated	Measured	Simulated
3-14-78	14	21	-	48	-
3-15-78	14	20	24	40	36
3-16-78	12	21	-	38	36
3-17-78	14	19	20	34	-
3-18-78	14	18	23	34	34

Table 5: Time of Minimum Temperature as a Function of Depth

	DEPTH					
Date	Surface Simulated	0.15 m (0.5 foot) Measured	0.33 m (1 foot) Simulated	0.66 m (2 foot) Measured		Simulated
3-14-78	-	8	-	35		-
3-15-78	6	10	14	28		22
3-16-78	2	10	12	24		-
3-17-78	8	8	13	26		24
3-18-78	6	8	14	21		22

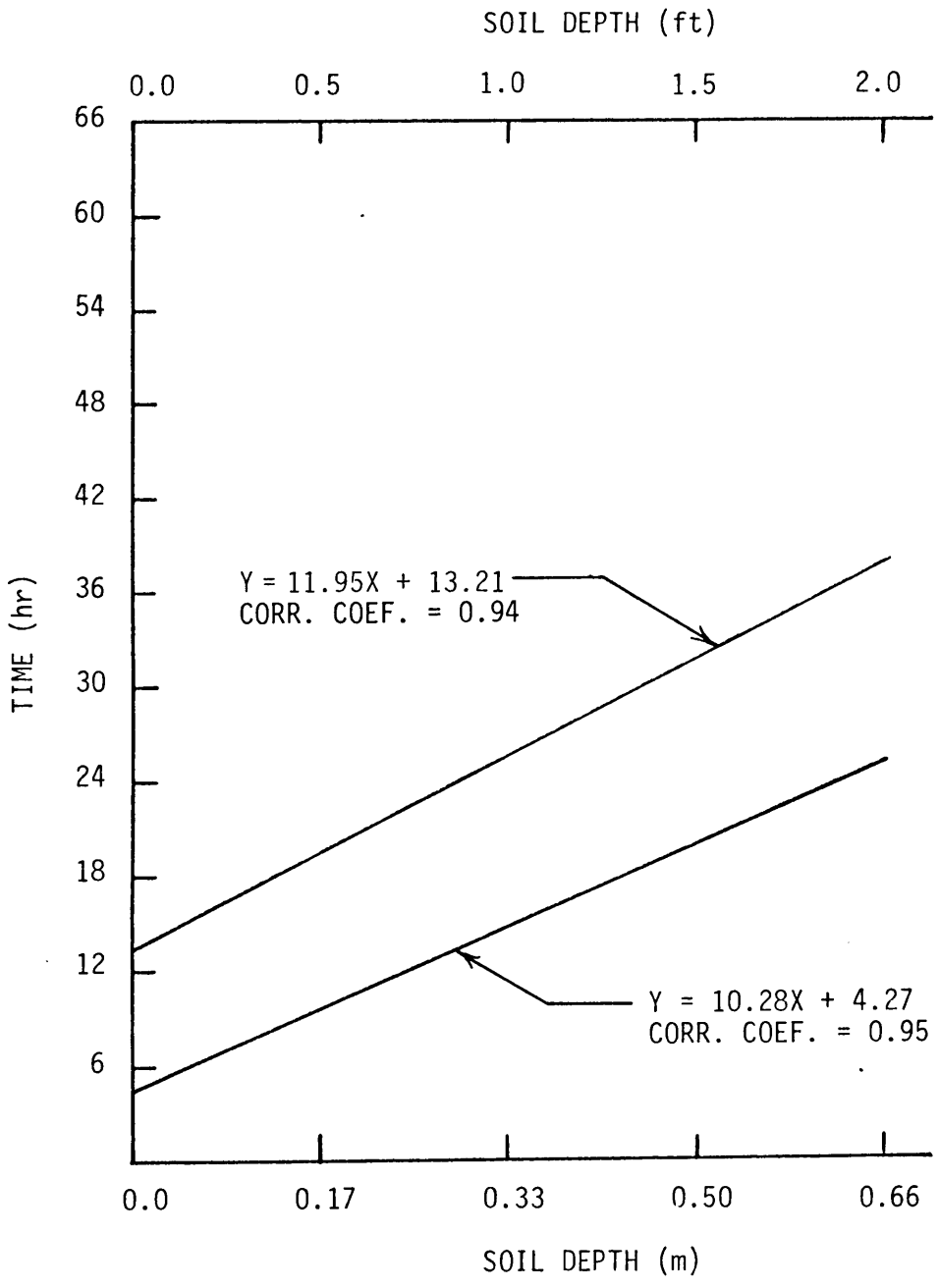

FIGURE 18 TIME TO TEMPERATURE MAXIMUM AND MINIMUM VS. SOIL DEPTH

The average simulated energy loss to the soil for the four days of test was 29.7 MJ/day (28.15 k BTU/day). Using power consumption measurements for the four-day period of March 14 to March 18, . 1978, which included the four-day simulation period, and the assumption of 10% of total energy loss for Pond 2 occurred to the soil (Holmes, Vaughan, and Bell, 1978), the average measured energy loss was 31.52 MJ/day (29.88 k BTU/day). Comparison of the simulated results with the measured results shows that simulated results are within 1.82 MJ/day (1.73 k BTU/day) or 5.8% of measured results.

Insulation Treatments Modeled

Since insulation of an energy storage pond can be done during pond construction or after the pond has been in use for some time, two insulation treatments were modeled. One treatment involved insulation of the ground-atmosphere interface to a distance of 0.33 m (1 ft) from the pond edge and also at a distance of 0.33 m (1 ft) from the pond edge to a depth of 0.66 m (2 ft). This treatement represents the case where insulation is installed after a pond has been in service for a period of time (Figure 19). Without draining the pond, a trench could be excavated around the pond's perimeter. This trench would be filled with insulation. The ground surface would be insulated and covered with a layer of soil for protection from traffic and the elements.

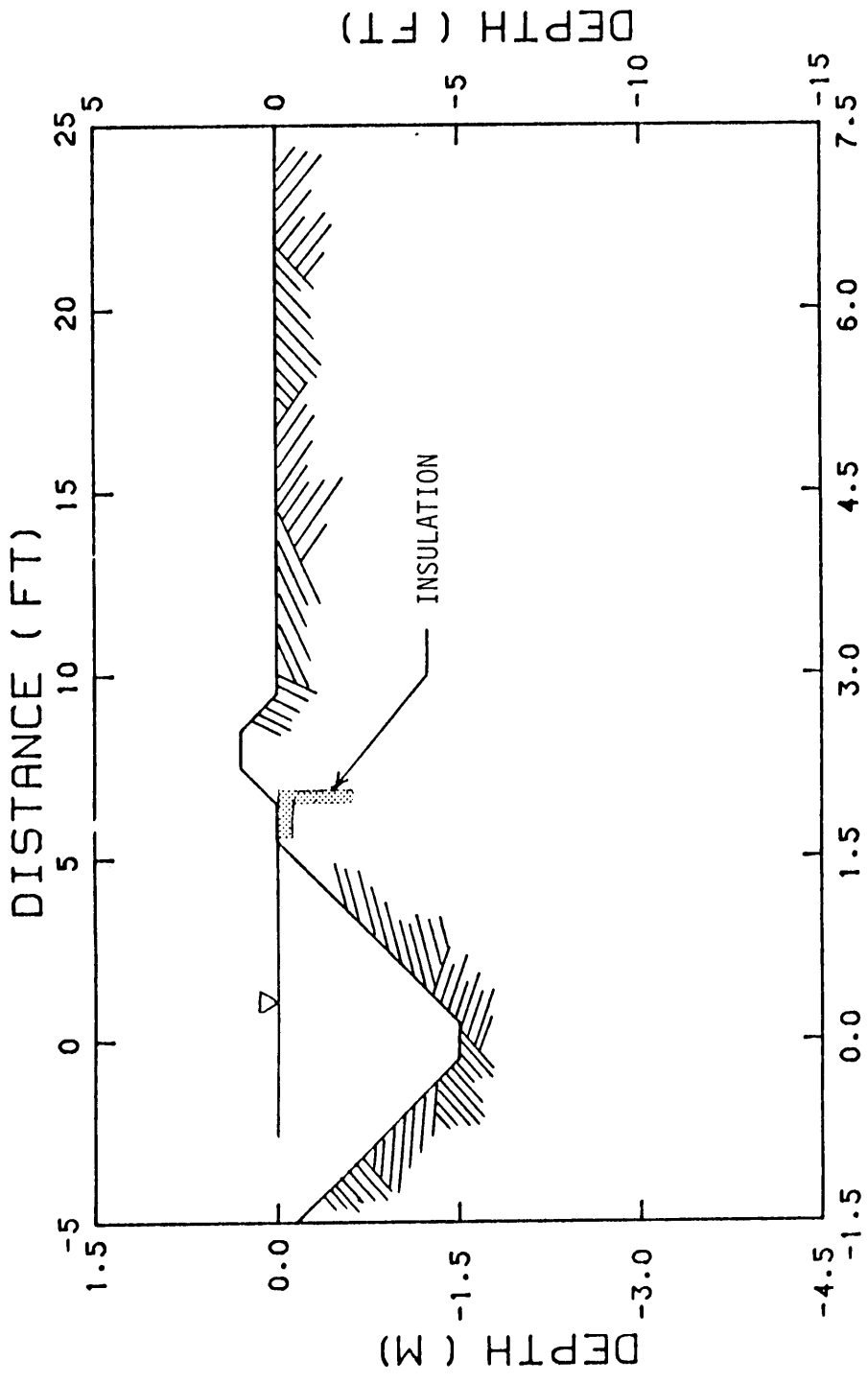

FIGURE 19 INSULATION TREATMENT - SOIL SURFACE

The second case modeled represents the insulation treatment that might be used when a pond is insulated during construction. In this case the ground surface comprising the pond banks and bottom are insulated prior to filling the pond with water or wastewater (Figure 20). Both treatments assume an impermeable water barrier is used to line the pond, thus eliminating heat loss by infiltration of warmed water into the soil. The insulation simulated in these tests had a conductivity of 99.7 J/h-m-^{o}C (0.016 BTU/h-ft-^{o}F) and a thickness of 0.10 m (0.33 ft) was employed. The results of the simulations are depicted in Figures 21 and 22 and summarized in Tables 6 and 7.

The average simulated energy loss to the soil from the pond insulated on sides and bottom for the four days of testing was 4.90 MJ/day (4.64 k BTU/day). Using power consumption measurements for the four-day period of March 14 to March 18, 1978, which includes the four-day simulation period, and the assumption that 30% of total energy loss occurring from pond 4 through the insulated pond sides and bottom (Holmes, Vaughan, and Bell, 1978), the average measured energy loss was 9.41 MJ/day (8.92 kBTU/day). Comparison of the simulated results with the measured results shows that simulated results underestimated measured results by 4.51 MJ/day (4.28 k BTU/day) which is 48% of the measured results.

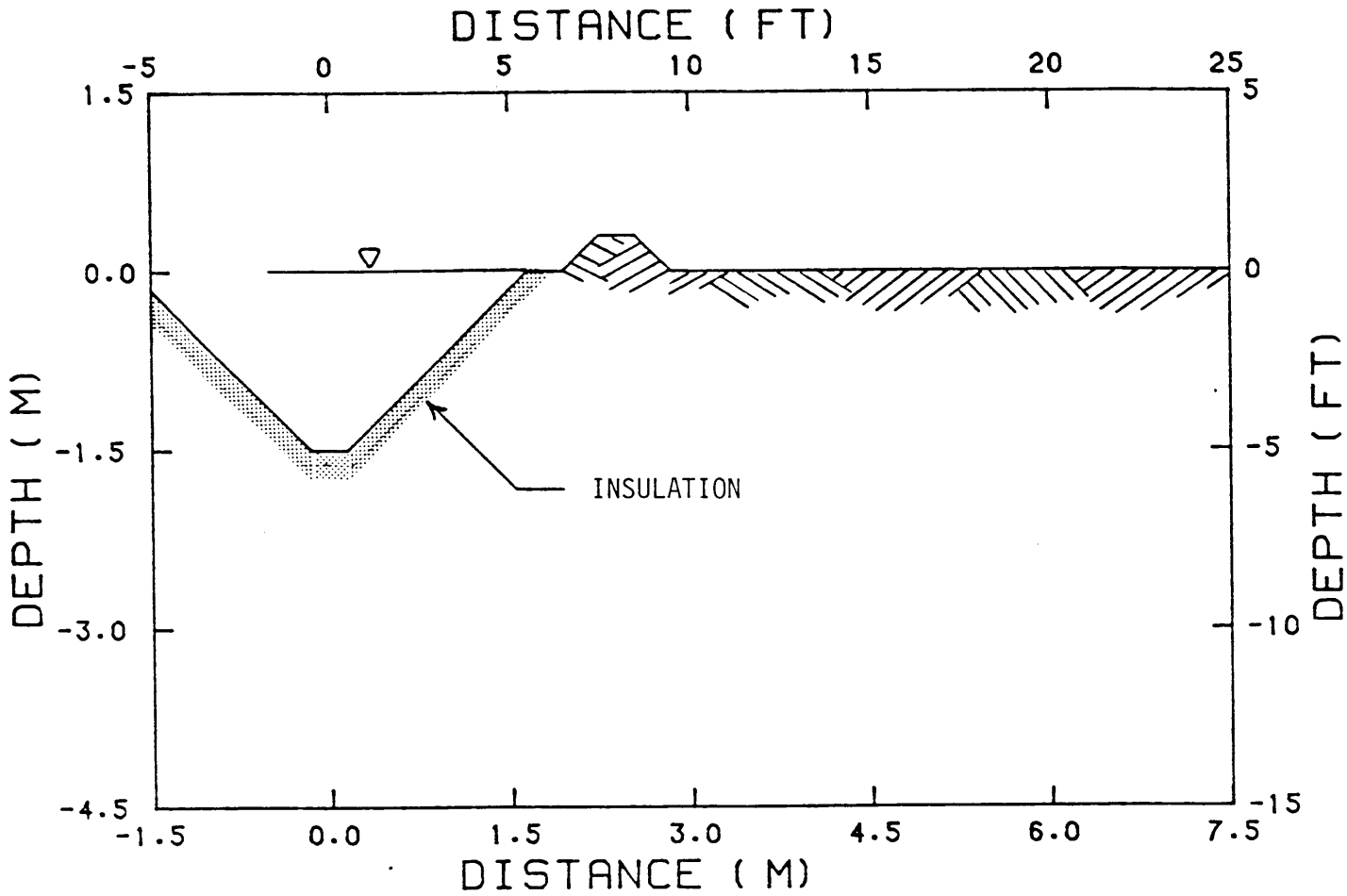

FIGURE 20 INSULATION TREATMENT - SIDES AND BOTTOM

Several explanations can be offered for the simulated results being less than measured results. The temperature distribution assumed may be one source of error. Soil temperatures were not measured in the vicinity of the insulated ponds, consequently, a temperature distribution for a pond with sides and bottom insulated was assumed for the simulation. An overestimation of soil temperature next to the insulation by only 2.8 ^{o}C (5 ^{o}F) could account for an underestimate of heat loss by about 1.12 MJ/day (1.08 k BTU/day).

Since the measured energy loss through the insulated pond sides and bottom were really an estimate, based on 30% of the total measured pond energy loss leaving by this mode, an overestimate of this mode of loss could produce a substantial error. For example, an assumption of 25% loss by this mode instead of the original assumption of 30% would result in an energy loss rate of 7.81 MJ/day (7.4 k BTU/day) compared to the 9.41 MJ/day (8.92 k BTU/day). A third explanation, possibly the most significant, is the presence of cracks in the insulation. The insulation used in the experiments consisted of 0.46 m x 0.91 m (1.5 ft x 3 ft) modules that were cut to fit the pond shape. The heat transferred by convection through these cracks was estimated to be 1.88 MJ/day (1.78 k BTU/day) when the following

assumptions were made:

1. crack area represents 4% of total pond wall area
2. convection heat transfer coefficient of 0.02 MJ/h-m^2-^{0}C (1 BTU/h-ft^2-^{0}F)
3. average temperature difference between soil and water of 5.6 ^{0}C (10 ^{0}F).

If these three conditions were to occur simultaneously, the discrepency between simulated and measured results would be almost totally explained.

From Figures 21 and 22 and Tables 6 and 7, it is apparent that insulation of the soil surface and in a trench of 0.66 m (2 ft) depth can demonstrate an energy savings of about 67% compared to the no insulation case. Insulation of the pond sides and bottom demonstrated an energy savings of about 84% compared to the case when no insulation was used.

The execution time for Program 4 required approximately 1 hour and 12 minutes for each day of simulated results, using a one-hour time increment. Consequently, testing of the program for more varied conditions of weather, pond water temperature, soil conductivity, or insulation characteristics would require much more computer time than was available.

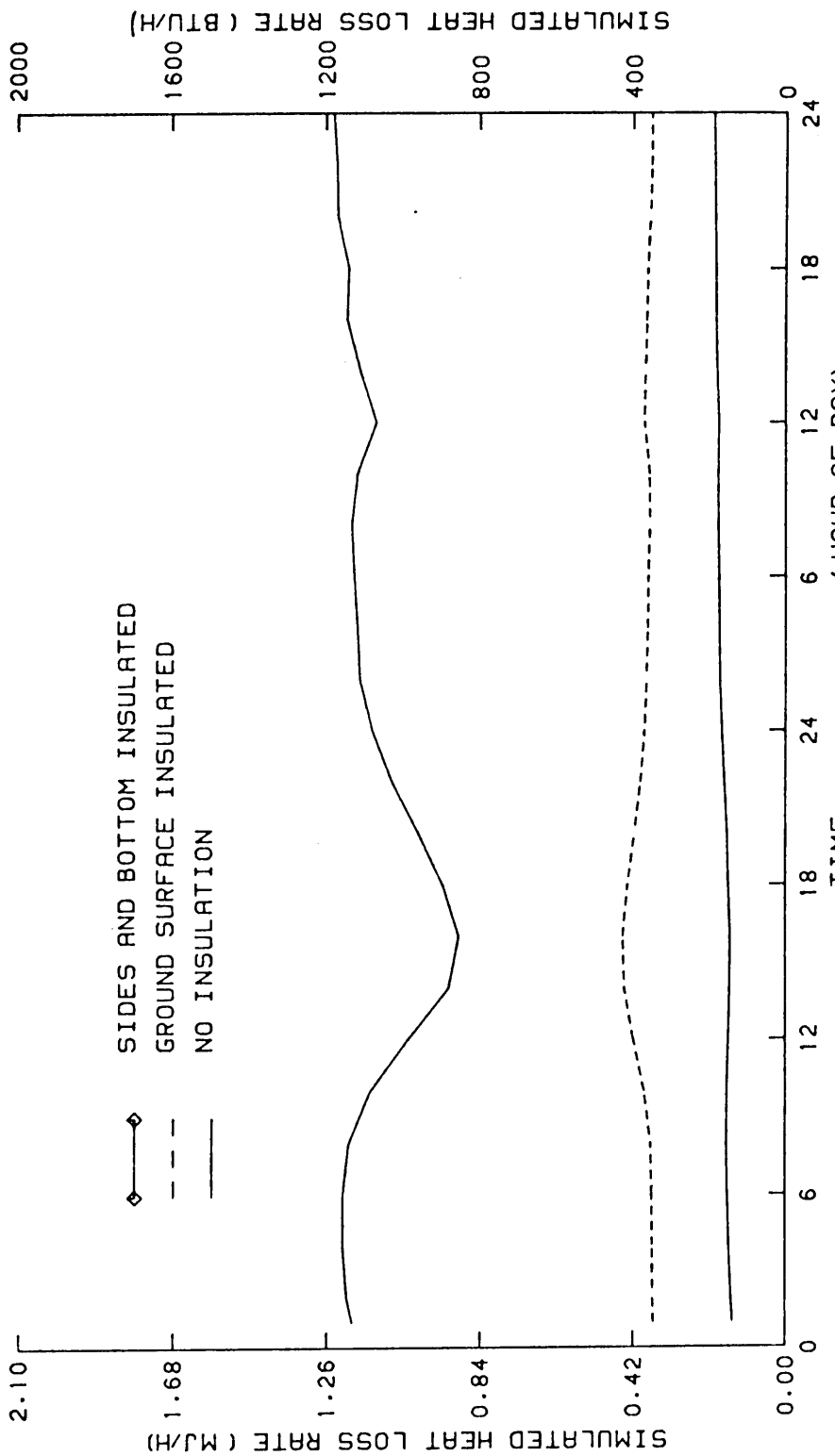

FIGURE 21 SIMULATED HEAT LOSS RATE VS TIME OF DAY
MARCH 15 AND 16, 1978

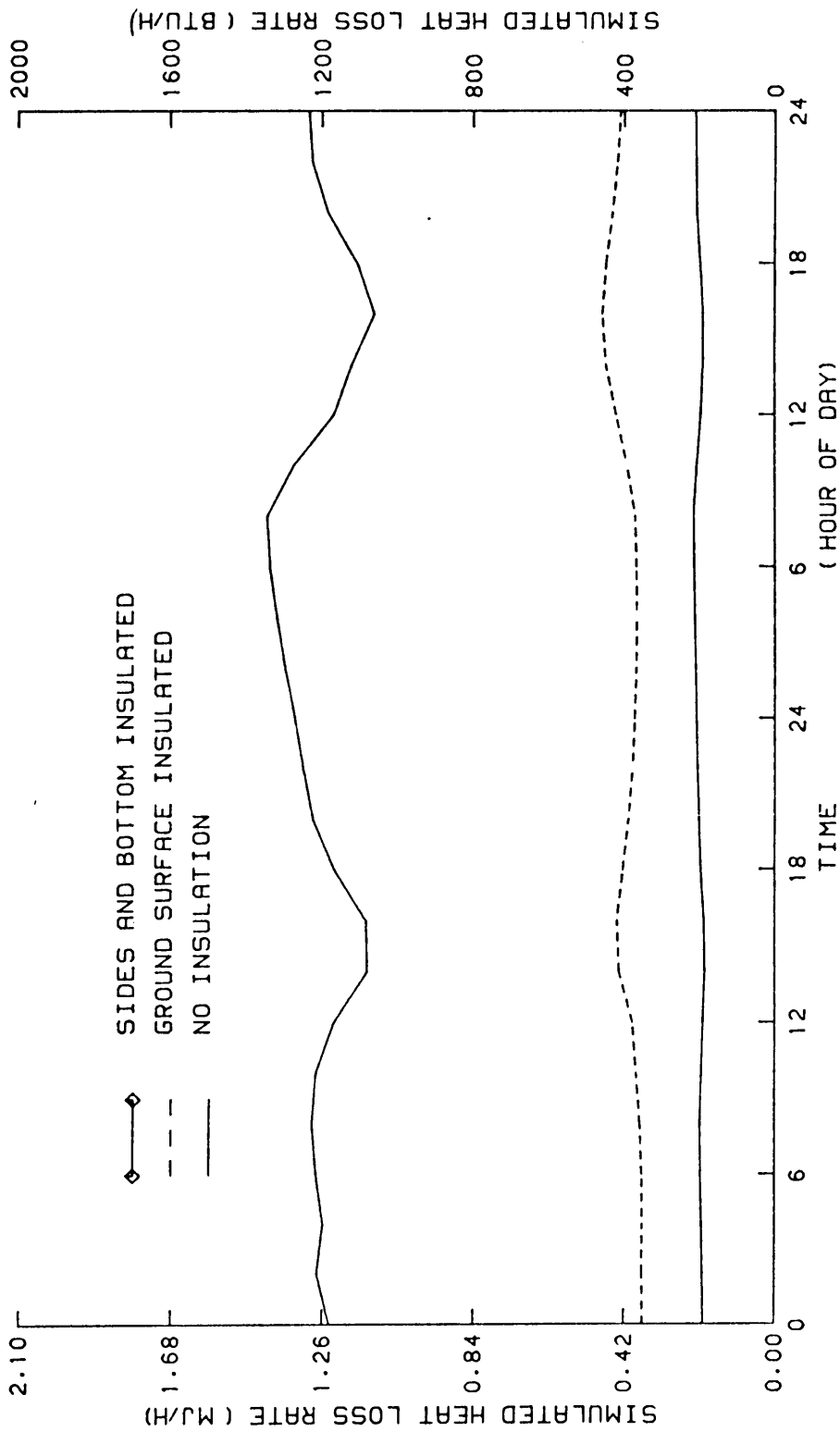

FIGURE 22 SIMULATED HEAT LOSS RATE VS TIME OF DAY
MARCH 17 AND 18, 1978

Table 6: Summary of Daily Simulated Energy Loss to the Soil

Date	Insulation Treatment: Uninsulated	Ground Surface Insulated	Pond Sides and Bottom Insulated
	MJ (k BTU)	MJ (k BTU)	MJ (k BTU)
3-15-78	26.15 (24.79)	9.65 (9.15)	3.85 (3.65)
3-16-78	25.48 (27.15)	9.11 (8.63)	4.55 (4.31)
3-17-78	30.04 (28.47)	9.58 (9.08)	4.97 (4.71)
3-18-78	30.93 (29.32)	10.31 (9.77)	5.21 (4.94)

Table 7: Comparison of Simulated Insulation Treatments to No Insulation

Date	Heat Loss Ratio Resulting from Insulation Treatment	
	Ground Surface Insulated / Uninsulated	Pond Sides and Bottom Insulated / Uninsulated
3-15-78	0.37	0.15
3-16-78	0.32	0.16
3-17-78	0.33	0.17
3-18-78	0.33	0.17

SUMMARY AND CONCLUSIONS

Energy losses from an energy storage pond were investigated. To simulate these energy losses, a three-dimensional finite element model was developed and implemented with the aid of a high speed digital computer. The model was capable of handling variations in weather conditons, storage pond water temperature and quantity and location of insulation that might be applied to the soil. Four warmed water storage ponds were constructed to provide initial conditions for the model and to verify model results.

The conclusions derived from the investigation are as follows:

1. The model predicted soil temperatures and responded in an appropriate manner to the boundary conditions applied. The long execution time on the computer limits the use of the model for studying the effects of a large number of input parameters. Excessive computer core memory requirements limit the model from being used with the most appropriate boundary conditions at some distance from the pond. The boundary conditions at the soil-atmosphere

interface were limited by available information on heat transfer by evaporation and convection from the soil.

2. The model predicted energy loss from the pond to the uninsulated soil within 5.8% of the measured energy losses. The model underestimated energy loss from the pond to the soil by 48% when the pond walls and bottom were insulated.

3. Based on the pond water temperatures assumed, energy loss to the soil from an uninsulated pond of the size investigated was of the order of magnitude of 26.4-31.7 MJ/day (25-30 k BTU/day).

4. Insulation of the soil-atmosphere interface and in a trench 0.66 m (2 ft) deep located 0.33 m (1 ft) from the pond edge reduced energy loss to the soil by 67% compared to the case where no insulation was used.

5. Insulation of the soil-water interface reduced energy loss to the soil by 84% compared to the no insulation case.

6. Based on conclusion number 4, it is apparent that much of the energy loss from a pond of this size and shape occurs as perimeter losses at the soil-atmosphere interface area near the pond edge.

7. Conclusions 4 and 5 are highly dependent upon insulation type and quantity being used and the weather conditions experienced by the pond and should, therefore, not be applied universally.

RECOMMENDATIONS

It is difficult to make general recommendations on how any particular energy storage pond should be insulated. Many factors, primarily economic, determine which alternatives should be pursued. Insulation of the energy storage pond surface is definitely beneficial as shown by Holmes, Vaughan, and Bell (1978). Insulation of the soil-atmosphere interface, even if just to minimize evaporation, can show appreciable savings. Therefore, it is recommended that this be seriously considered in any design as the minimal insulation for an energy storage pond.

Methods besides insulation are available for reducing energy loss from an energy storage pond. Appropriate vegetation planted in the vicinity of the pond could reduce convection heat loss by reducing wind speed. Net long wave radiative heat loss could be reduced by the vegetation as it shades the soil from exposure to a low temperature sky. After a period of time, vegetative debris could accumulate on the ground producing an insulating layer. Mechanical structures could be constructed to reduce convection losses. Examples of this might include wind breaks and covers that extend beyond the pond surface boundary. Snow acts as an

insulating material. Appropriately placed snow fences would cause snow to be deposited around the pond, thus providing temporary insulation during the coldest periods of the year.

Observation of the results produced by the various soil-atmosphere interface boundary condition models indicates that evaporation energy loss can account for as much as 30-50% of the total energy lost from this boundary when the soil surface is not frozen. One technique for reducing evaporation from this surface which might be accomplished rather inexpensively and with appreciable energy savings is to use a plastic vapor barrier covered by a layer of coarse material such as rocks. The rocks would drain quickly preventing water from being available for evaporation, and would also protect the plastic vapor barrier from degradation. The vapor barrier would prevent moisture from entering the evaporation zone by capillary action and would prevent excess surface water from passing through the warmed soil zone resulting in energy movement away from the zone by convection.

The computer program developed to implement the model could have other applications in addition to the study of energy loss from a solar energy storage pond. One use might include the study of energy loss from heated below-grade builds or basements. With some modifications, the model

could be used to study heat loss to the soil from buildings constructed without basements.

The model could be used for further investigation of the effect of increased storage pond temperatures and quantities of insulation used as well as the effect of more extreme weather conditions. Because very little information was available about convection and evaporation heat losses from the soil surface under winter conditions, more research should be conducted in these areas.

BIBLIOGRAPHY

1. Alpert, J. E. et. al. 1976. Soil temperatures and heat loss for a hot water pipe network buried in irrigated soil. Journal of Environmental Quality, 5(4).

2. American Society of Heating, Refrigerating, and Air-Conditioning Engineers (ASHRAE). 1977. ASHRAE Handbook 1977 Fundamentals. New York.

3. Amos, D. 1979. Personal Communications. Agronomy Department, VPI and SU.

4. Aral, M. M., P. G. Mayer, and C. V. Smith, Jr. 1973. Finite element Galerkin method solutions to selected elliptic and parabolic differential equations. Proceedings of the Third Conference on Matrix Methods in Structural Mechanics, Part 1. Wright-Patterson Air Force Base, Ohio, December.

5. Beard, J. T. et. al. 1977. Annual collection and storage of solar energy for the heating of buildings. Annual Progress Report, May 1976-July 1977.

6. Beard, T. J. and D. K. Hollen. 1969. The Influence of Solar Radiation Reflectance on Water Evaporation; Bulletin 30. Water Resources Research Center, Virginia Polytechnic Institute, Blacksburg, VA.

7. Beckett, R. E. and S. C. Chu. 1973. Finite element method applied to heat conduction in solids with non-linear boundary conditions. Journal of Heat Transfer, Vol. 95.

8. Bolz, R. E. and G. L. Tuve, eds. 1970. Handbook of Tables for Applied Engineering Science. The Chemical Rubber Co., Cleveland, OH.

9. Bonacina, C., G. Comini, A. Fasano, and M. Primicerio. 1973. Numerical solution of phse-change problems. International Journal of Heat and Mass Transfer, Vol. 16.

10. Brooker, D. B. 1967. Mathematical model of the psychrometric chart. Trans. ASAE 10(4).

11. Brooker, D. B., F. J. Bakker-Arkema, and C. W. Hall. 1974. Drying Cereal Grains. AVI Publishing Co., Inc., Westport, CT.

12. Brown, K. W. and N. J. Rosenberg. 1973. A resistance model to predict evapotranspiration and its application to a sugar beet field. Agronomy Journal 65(3).

13. Byers, H. R. 1959. General Meteorology, third edition. McGraw-Hill Book Co., Inc., New York.

14. Carnaham, B., H. A. Luther, and J. O. Wilkes. 1969. Applied Numerical Methods. John Wiley and Sons, Inc., New York.

15. Carslaw, H. S. and J. C. Jaeger. 1957. Conduction of Heat in Solids. Oxford University Press.

16. Chapman, A. J. 1974. Heat Transfer. McMillian Publishing Co., Inc., New York.

17. Chudnovskii, A. F. 1962. Heat Transfer in the Soil. National Science Foundation, Washington, DC, by Israel Program for Scientific Translations, Jerusalem.

18. Comini, G. and S. Del Guidice. 1974. Finite element solution of non-linear heat conduction problems with special reference to phase change. International Journal for Numerical Methods in Engineering, Vol. 8.

19. Council for Agricultural Science and Technology (CAST). 1977. Energy use in agriculture: now and in the future. Report No. 68. CAST Headquarters Office: Agronomy Bldg., Iowa State University, Ames, IA 50011.

20. Crowe, P. R. 1971. Concepts in Climatology. Longman Group, Ltd., London.

21. Davis, B. W., J. A. Day, and A. Iantuono. A generalized numerical model for predicting energy transfers and performance of large solar ponds. Sharing the Sun! Solar Technology in the Seventies, Vol. 5. The American Section of the International Solar Energy Society, Cape Canaveral, FL.

22. deVries, D. A. and N. H. Afgan. 1975. Heat and Mass Transfer in the Biosphere, Part 1: Transfer Processes in Plant Environment. John Wiley and Sons, New York.

23. Duffie, J. A. and W. A. Beckman. 1974. Solar Energy - Thermal Processes. John Wiley and Sons, Inc., New York.

24. Dusinberre, G. M. 1949. Numerical Analysis of Heat Flow. McGraw-Hill Book Co., Inc., New York.

25. Eagleson, P. S. 1970. Dynamic Hydrology. McGraw-Hill Book Co., New York.

26. Eckert, E. R. G. and R. M. Drake, Jr. 1959. Heat and Mass Transfer. McGraw-Hill Book Co., New York.

27. Emery, A. F. and W. W. Carson. 1971. An evaluation of the use of the finite-element method in the computation of temperature. Journal of Heat Transfer: Transactions of the ASME, Vol. 93, Series C(2), May.

28. Fisher, R. C. and A. D. Ziebur. 1975. Calculus and Analytic Geometry, third edition. Prentice-Hall, Inc., Englewood Cliffs, NJ.

29. Gallagher, R. H. and R. H. Mallett. 1971. Efficient solution process for finite element analysis of transient heat conduction. Journal of Heat Transfer - Transactions of ASME, Vol. 93, Series C(3).

30. General Electric Co. 1970. Heat Transfer and Fluid Flow Data Book. Research and Development Center, Schenectady, New York.

31. Griffith, M. V. and E. E. Hutchings. 1951. Some practical applications of heat transfer between burried objects and the soil. Proceedings of the General Discussion of Heat Transfer, September. Institution of Mechanical Engineers, London.

32. Hildebrand, F. B. 1976. Advanced Calculus for Applications, second edition. Prentice-Hall, Inc., Englewood Cliffs, NJ.

33. Hillel, D. 1971. Soil and Water - Physical Principles and Processes. Academic Press, New York.

34. Holmes, B. J., D. H. Vaughan, and E. S. Bell. 1978. Evaluation of low-cost thermal storage ponds for solar heat. ASAE Paper No. 78-3503. American Society of Agricultural Engineers, St. Joseph, MI.

35. Huebner, K. H. 1975. The Finite Element Method for Engineers. John Wiley and Sons, Inc., New York.

36. Ingersoll, L. R., Zobel, O. J., and A. C. Ingersoll. 1948. Heat Conduction with Engineering Applications. McGraw-Hill Book Co., Inc., New York.

37. Ioffe, A. F. and I. B. Revut, eds. 1966. Fundamentals of Agrophysics. Israel Program for Scientific Translations, Ltd.

38. Irons, B. M. 1969. Economical computer techniques for numerically integrated finite elements. International Journal for Numerical Methods in Engineering, Vol. 1.

39. Jacob, M. 1949. Heat Transfer - Vol. 1. Wiley and Sons, Inc., New York.

40. Kersten, M. S. 1949. Thermal properties of soils. University of Minnesota Engineering Experiment Station; Bulletin 28.

41. Kikuchi, F. and Y. Ando. 1973. A finite element method for various kinds of initial value problems. Proceedings of the Third Conference on Matrix Methods in Structural Mechanics, Part 1. Wright-Patterson Air Force Base, Ohio, December.

42. Kirkham, D. and W. L. Powers. 1972. Advanced Soil Physics. Wiley-Interscience, John Wiley and Sons, Inc.

43. Kohnke, H. 1968. Soil Physics. McGraw-Hill Book Co., New York.

44. Kreith, F. 1965. Principles of Heat Transfer, second edition. International Textbook Co., Scranton, PA.

45. Lee, W. H. K. 1965. Terrestrial heat flow. Geophysical Monograph Series, No. 8. American Geophysical Union of the National Academy of Sciences - National Research Council Publication No. 1288.

46. Luikov, A. V. 1961. Heat and Mass Transfer in Capillary-Porous Bodies. Pergamon Press, Ltd., New York.

47. Mandarov, A. A. 1976. Relationship between grassland surface temperature and air temperature in the summertime. Heat Transfer - Soviet Research, 8(2), March-April.

48. Mather, J. R. 1974. Climatology: Fundamentals and Applications. McGraw-Hill, Inc., New York.

49. Misra, R. N. and H. M. Keener. 1978. Solar grain drying for Ohio solar grain drying proceedings. Publication No. Conf-7805129. Purdue University, U.S. Department of Energy and USDA.

50. Mizumachi, W. . 1973. Non-linear thermal stress analysis for nuclear power plant by finite element method. Proceedings of the Third Conference on Matrix Methods in Strutural Mechanics. Wright-Patterson Air Force Base, Ohio, December.

51. Nielson, C. E. 1976. Experience with a prototype solar pond for space heating. Sharing the Sun! Solar Technology in the Seventies, Vol. 5. The American Section of the International Solar Energy Society, Cape Canaveral, FL.

52. Oden, J. T. 1969. A general theory of finite elements I: Topological considerations. International Journal of Numerical Methods in Engineering, 1(3).

53. Oden, J. T. 1969. A general theory of finite elements II: Applications. International Journal of Numerical Methods in Engineering, 1(3).

54. Ozisic, M. N. 1968. Boundary Value Problems of Heat Conduction. International Textbook Company, Scranton, PA.

55. Paily, P. P., E. O. Macagno, and J. F. Kennedy. 1974. Winter-Regime Surface Heat Loss from Heated Streams. Institute of Hydraulic Research. University of Iowa, Iowa City, IA, March.

56. Pinder, G. F. and W. G. Gray. 1977. Finite Element Simulation in Surface and Subsurface Hydrology. Academic Press, New York.

57. Purcell, E. J. 1965. Calculus with Analytic Geometry. Appleton-Century-Crofts, New York.

58. Rasponin, G. A. 1974. Transfer of heat from water surfaces to the atmosphere. Heat Transfer - Soviet Research, 6(4), July-August.

59. Reiter, M. A. 1969. Terrestrial Heat Flow and Thermal Conductivity in Southwestern Virginia. Ph.D. Thesis, VPI & SU, Blacksburg, VA.

60. Rohsenow, W. M. and J. P. Hartnet. 1973. Handbook of Heat Transfer. McGraw-Hill Book Co., New York.

61. Rosenberg, N. J. 1974. Microclimate: The Biological Environment. John Wiley and Sons, Inc., New York.

62. Seagrave, R. C. 1971. Biomedical Applications of Heat and Mass Transfer. Iowa State University, Ames, IA.

63. Segerlind, L. J. 1976. Applied Finite Element Analysis. John Wiley and Sons, Inc., New York.

64. Shelton, J. 1975. Underground storage of heat in solar heating systems. Solar Energy, 17(2).

65. Short, T. H., W. L. Roller, and P. C. Badger. 1976. A solar pond for heating greenhouses and rural residences - a preliminary report. ASAE Paper No. 76-4012.

66. Simpson, G. C. 1928. Memoirs of the Royal Meteorological Society 3(21). London.

67. Snider, D. M. and R. Viskanta. 1975. Radiation induced thermal stratification in surface layers of stagnant water. Journal of Heat Transfer: Transactions of the ASME, Vol. 97, Series C(1), February.

68. Stickford, G. H. Jr., C. F. Holt, and G. R. Whitacre. 1976. An analysis of buried heat storage tank losses. Sharing the Sun, Solar Technology in the Seventies, Vol. 10. American Section, International Solar Energy Society, Cape Canaveral, FL.

69. Sutton, O. G. 1953. Micrometeorology. McGraw-Hill Book Co., Inc., New York.

70. Swet, C. J. 1976. New directions in heat storage for buildings. Sharing the Sun! Solar Technology in the Seventies, Vol. 8. The American Section of the International Solar Energy Society, Cape Canaveral, FL.

71. Tanayeva, S. A. 1974. Thermal conductivity of moist bulk materials. Heat Transfer - Soviet Research, 6(2), March - April.

72. Tye, R. P. 1969. Thermal Conductivity: Vol. 1. Academic Press, New York.

73. U.S. Department of Agriculture. 1976. Energy and U.S. Agriculture: 1974 Data Base. Vol. 1 Federal Energy Administration FEA/D-76/459.

74. U.S. Dept. of Commerce - National Oceanic and Atmospheric Administration (NOAA). 1978. Local Climatological Data - Monthly Summary. National Climatic Center, Asheville, NC.

75. Van Wijk, W. R., ed. 1976. Physics of Plant Environment, 2nd edition. Noth-Holland Publishing Co., Amsterdam.

76. Vaughan, D. H. 1972. Thermocouple Sensing of Soil Temperature from a Moving Vehicle. Unpublished Ph.D. thesis, University of North Carolina - Raleigh.

77. Votyakova, N. I. 1976. Evaluation of equations for calculation of depth of seasonal freezing or thawing of soil. Heat Transfer - Soviet Research, 8(2), March-April.

78. Williams, J. R. 1976. Solar Energy Technology and Applications: 1976 Solar Update. Ann Arbor Science Publishers, Inc., Ann Arbor, Michigan.

79. Yasinsky, J. B. 1971. The solution of three-dimensional composite media heat conduction problems by synthesis methods. Journal of Heat Transfer: Transactions of the ASME, Vol. 93, Series C(2), May.

80. Yong, R. N. and B. P. Warkentin. 1966. Introduction to Soil Behavior. the McMillian Co., New York.

81. Zienkiewicz, O. C. 1971. The Finite Element Method in Engineering Science. McGraw-Hill Book Co., London.

82. Zienkiewicz, O. C. and C. J. Parekh. 1970. Transient field problems: two-dimensional and three-dimensional analysis by isoparametric finite elements. International Journal for Numerical Methods in Engineering, Vol. 2.

APPENDIX

The Finite Element Method

Many problems can be specified with differential equations which describe the behavior of an infinitesimal region or with a variational principle valid over the entire region. In the second case, the correct solution is one which minimizes some functional (I) defined by integration of the unknown quantities over the domain. Both methods are equivalent (Zienkiewicz, 1971).

The differential equation describing a physical system is always written as a function of an unknown quantity $\{\phi\}$ and its derivatives. The function is defined as an integral over the domain (V) and its boundary (S) such that:

$$I = \int_V f\left(\{\phi\}, \frac{\partial\{\phi\}}{\partial x} \ldots\right) dV + \int_S g\left(\{\phi\}, \frac{\partial\{\phi\}}{\partial x} \ldots\right) dS \qquad [A-1]$$

V = volume in three dimensions

S = surface in three dimensions

"The fundamental concept of the finite element method is that any continuous quantity,..., can be approximated by a discrete model composed of a set of piecewise continuous functions defined over a finite number of subdomains" (Segerlind, 1976). The spacial subdomains are called

elements and each element is delineated by the position of several points within the domain. The continuous function $\{\phi\}$ is defined by its value at a finite number of these points or nodes. The equation for the continuous function within an element is called an interpolation function and can be written as:

$$\{\phi\} = \lfloor N \rfloor \{\phi\}^e \qquad [A-2]$$

$\lfloor N \rfloor$ = shape function of coordinates

$\{\phi\}^e$ = values of the function $\{\phi\}$ at the nodes or $\begin{Bmatrix} \Phi_1 \\ \Phi_2 \\ \vdots \\ \Phi_n \end{Bmatrix}$

For the functional I to be minimized over the whole domain,

the following relationship must hold:

$$\frac{\partial I}{\partial \{\Phi\}} = \begin{Bmatrix} \frac{\partial I}{\partial \{\Phi\}_1} \\ \frac{\partial I}{\partial \{\Phi\}_2} \\ \vdots \\ \frac{\partial I}{\partial \{\Phi\}_n} \end{Bmatrix} = 0 \qquad [A-3]$$

n = total number of different parameters

The element derivatives of the function can be written in a linear form as:

$$\frac{\partial I^e}{\partial \{\Phi\}^e} = [k]^e \{\Phi\}^e + \{F\}^e \qquad [A-4]$$

$[k]^e$ = square matrix of influence coefficients (stiffness matrix)

$\{F\}^e$ = vector of resultant nodal actions (force vector)

The equation to be minimized over the whole domain can be

written as:

$$\frac{\partial I}{\partial \{\phi\}} = [K]\{\phi\} + \{F\} = 0 \qquad [A\text{-}5]$$

$$[K_{ij}] = \sum [k_{ij}]^e \qquad [A\text{-}6]$$

$$\{F_i\} = \sum \{F_i\}^e \qquad [A\text{-}7]$$

i = row number designation

j = column number designation

An element in three dimensions can be described as a tetrahedron, right prism, or general hexahedron. In this work tetrehedral elements were used. The four nodes of the tetrahedron can be characterized by the subscripts i, j, k, and l. The linear interpolation polynomial for the tetrahedral element is defined as:

$$\{\phi\} = \alpha_1 + \alpha_2 x + \alpha_3 y + \alpha_4 z \qquad [A\text{-}8]$$

In the case of the tetrahedral element, the coefficients (α)

are established by the following set of equations:

$$\begin{aligned}
\Phi_i &= \alpha_1 + \alpha_2 X_i + \alpha_3 Y_i + \alpha_4 Z_i \\
\Phi_j &= \alpha_1 + \alpha_2 X_j + \alpha_3 Y_j + \alpha_4 Z_j \\
\Phi_k &= \alpha_1 + \alpha_2 X_k + \alpha_3 Y_k + \alpha_4 Z_k \\
\Phi_l &= \alpha_1 + \alpha_2 X_l + \alpha_3 Y_l + \alpha_4 Z_l
\end{aligned} \qquad [A\text{-}9]$$

where X_i, Y_i, Z_i refer to the x, y, z coordinates of the i-th node and Φ_i refers to the value of the interpolation function at the i-th node, etc. These equations can be written more concisely as:

$$\{\Phi\} = [M] \begin{Bmatrix} \alpha_1 \\ \alpha_2 \\ \alpha_3 \\ \alpha_4 \end{Bmatrix} \qquad [A\text{-}10]$$

$$\{\Phi\}^T = [\Phi_i \ \Phi_j \ \Phi_k \ \Phi_l] \qquad [A\text{-}11]$$

$$[M] = \begin{bmatrix} 1 & X_i & Y_i & Z_i \\ 1 & X_j & Y_j & Z_j \\ 1 & X_k & Y_k & Z_k \\ 1 & X_l & Y_l & Z_l \end{bmatrix}$$

The vector $\{\alpha\}$ can be described in terms of the nodal values of $\{\Phi\}$ as

$$\{\alpha\} = [M]^{-1} \{\Phi\} \quad . \qquad [A-12]$$

It should be noted that the determinant of $[M]$ is six times the volume of the tetrahedral element or:

$$6V = |M| \qquad [A-13]$$

and the inverse of $[M]$ is obtained as

$$[M]^{-1} = \frac{1}{6V} \begin{bmatrix} a_i & b_i & c_i & d_i \\ a_j & b_j & c_j & d_j \\ a_k & b_k & c_k & d_k \\ a_l & b_l & c_l & d_l \end{bmatrix} \qquad [A-14]$$

When the nodes of the tetrahedral element are labeled counterclockwise looking at them from node 1, the elements in the matrix of equation [A-14] can be obtained by the co-factors of $|M|$, namely:

$$a_i = + \begin{vmatrix} X_j & Y_j & Z_j \\ X_k & Y_k & Z_k \\ X_l & Y_l & Z_l \end{vmatrix} \qquad b_i = - \begin{vmatrix} 1 & Y_j & Z_j \\ 1 & Y_k & Z_k \\ 1 & Y_l & Z_l \end{vmatrix}$$

$$c_i = - \begin{vmatrix} X_j & 1 & Z_j \\ X_k & 1 & Z_k \\ X_l & 1 & Z_l \end{vmatrix} \qquad d_i = - \begin{vmatrix} X_j & Y_j & 1 \\ X_k & Y_k & 1 \\ X_l & Y_l & 1 \end{vmatrix}$$

$$a_j = + \begin{vmatrix} X_i & Y_i & Z_i \\ X_k & Y_k & Z_k \\ X_l & Y_l & Z_l \end{vmatrix} \qquad b_j = + \begin{vmatrix} 1 & Y_i & Z_i \\ 1 & Y_k & Z_k \\ 1 & Y_l & Z_l \end{vmatrix}$$

$$c_j = + \begin{vmatrix} X_i & 1 & Z_i \\ X_k & 1 & Z_k \\ X_l & 1 & Z_l \end{vmatrix} \qquad d_j = + \begin{vmatrix} X_i & Y_i & 1 \\ X_k & Y_k & 1 \\ X_l & Y_l & 1 \end{vmatrix}$$

etc. with the sign on the cofactor alternating with row. Substituting [A-12] into [A-8] yields the equation for the interpolation function:

$$\phi = [1 \; x \; y \; z] \, [M]^{-1} \, \{\Phi\} \; . \qquad [A-15]$$

The shape function is therefore:

$$[N] = [1 \; x \; y \; z] \, [M]^{-1} \qquad [A-16]$$

and now the general function ϕ can be expressed within the domain of the element in terms of the values of $\{\phi\}$ at the nodes of the element namely $\{\Phi\}$.

To solve for the unknown values of Φ at the nodes, the equations for each element must be solved simultaneously. This is accomplished by combining the elemental equations into a set of linear simultaneous equations that are of the form of equation [A-5]. The process of forming the simultaneous equations is known as "assembling" because the process can be thought of as appropriately combining or "assembling" the finite elements to form the complete domain being modeled. A small example of how this is accomplished will be helpful in understanding the process. If a domain is discretized into two tetrahedral elements with five nodes, the following set of elemental equations may be written with the subscripts being the node number of the elements:

$$\begin{bmatrix} k_{11} & k_{12} & k_{13} & k_{14} \\ k_{21} & k_{22} & k_{23} & k_{24} \\ k_{31} & k_{32} & k_{33} & k_{34} \\ k_{41} & k_{42} & k_{43} & k_{44} \end{bmatrix} \begin{Bmatrix} \Phi_1 \\ \Phi_2 \\ \Phi_3 \\ \Phi_4 \end{Bmatrix} + \begin{Bmatrix} F_1 \\ F_2 \\ F_3 \\ F_4 \end{Bmatrix} = 0$$

[A-17]

$$\begin{bmatrix} k_{22} & k_{23} & k_{24} & k_{25} \\ k_{32} & k_{33} & k_{34} & k_{35} \\ k_{42} & k_{43} & k_{44} & k_{45} \\ k_{52} & k_{53} & k_{54} & k_{55} \end{bmatrix} \begin{Bmatrix} \Phi_2 \\ \Phi_3 \\ \Phi_4 \\ \Phi_5 \end{Bmatrix} + \begin{Bmatrix} F_2 \\ F_3 \\ F_4 \\ F_5 \end{Bmatrix} = 0$$

The "assembled" equation then appear as:

$$\begin{bmatrix} k_{11} & k_{12} & k_{13} & k_{14} & 0 \\ k_{21} & (k_{22} + k_{22}) & (k_{23} + k_{23}) & k_{24} & k_{25} \\ k_{31} & (k_{32} + k_{32}) & (k_{33} + k_{33}) & (k_{34} + k_{34}) & k_{35} \\ k_{41} & (k_{42} + k_{42}) & (k_{43} + k_{43}) & (k_{44} + k_{44}) & k_{45} \\ 0 & k_{52} & k_{53} & k_{54} & k_{55} \end{bmatrix} \begin{Bmatrix} \Phi_1 \\ \Phi_2 \\ \Phi_3 \\ \Phi_4 \\ \Phi_5 \end{Bmatrix} = \begin{Bmatrix} F_1 \\ F_2 \\ F_3 \\ F_4 \\ F_5 \end{Bmatrix}$$

[A-18]

When the boundary conditions are applied, this set of simultaneous linear equations can be solved for the unknown values of the function $\{\Phi\}$ at the nodes. One method of applying the boundary conditions to this set of equations is as follows. If Φ_1 is a known value of the function at node one, say it is B_1, then the main diagonal element of

the [K] matrix can be multiplied by a large number say 10^{15} and the corresponding element in the force vector can be replaced by $B_1 K_{11} \times 10^{15}$ producing the following set of equations.

$$\begin{bmatrix} K_{11} \times 10^{15} & K_{12} & K_{13} & K_{14} & 0 \\ K_{21} & K_{22} & K_{23} & K_{24} & K_{25} \\ K_{31} & K_{32} & K_{33} & K_{34} & K_{35} \\ K_{41} & K_{42} & K_{43} & K_{44} & K_{45} \\ 0 & K_{52} & K_{53} & K_{54} & K_{55} \end{bmatrix} \begin{Bmatrix} \Phi_1 \\ \Phi_2 \\ \Phi_3 \\ \Phi_4 \\ \Phi_5 \end{Bmatrix} = - \begin{Bmatrix} B_1 K_{11} \times 10^{15} \\ F_2 \\ F_3 \\ F_4 \\ F_5 \end{Bmatrix} \quad [A-19]$$

Since $K_{11} \times 10^{15}$ is so much greater than K_{12}, K_{13}, or K_{14}, solution of the set of equations will produce a value for $\Phi_1 = B_1$.

The vita has been removed from the scanned document

ENERGY LOSS TO THE SOIL SURROUNDING A BELOW GRADE SOLAR ENERGY STORAGE POND

by

Brian James Holmes

(ABSTRACT)

Several techniques have been proposed for storing collected solar energy. A study was undertaken to investigate energy losses to the soil surrounding a below grade solar energy storage pond. A three dimensional finite element model was developed to approximate the solution of the differential equation of heat transfer. The Crank-Nicholson central difference scheme was used to solve for the time derivative.

Four small ponds were constructed at the VPI & SU Swine Center, Blacksburg, Virginia, to study the effect of insulation on heat losses from a warmed water pond. The water in each pond was warmed with an electric resistance immersion heater. The power consumed by each heater was metered. The uninsulated (control) pond was more thoroughly

instrumented with thermocouples than were the other three ponds. These thermocouples provided data that were used as input to the computer model as well as data to verify the model.

Based on the conditions under which the model was tested, energy losses to the soil from an uninsulated pond were on the order of 26.4-31.7 MJ/day (25-30 k BTU/day). By providing insulation to the ground surface and to a depth of 0.66 m (2 ft) at a distance of 0.33 m (1 ft) from the pond edge, energy loss to the soil was reduced to about 33 percent of the uninsulated case. Insulation of the pond sides and bottom resulted in energy losses that were about 16 percent of those for the uninsulated pond.